



ELSEVIER

Contents lists available at [ScienceDirect](https://www.sciencedirect.com)

## International Journal of Plasticity

journal homepage: [www.elsevier.com/locate/ijplas](http://www.elsevier.com/locate/ijplas)

# History and temperature dependent cyclic crystal plasticity model with material-invariant parameters

Farhan Ashraf, Gustavo M. Castelluccio<sup>\*</sup>

School of Aerospace, Transport and Manufacturing, Cranfield University, Bedfordshire MK43 0AL, UK

## ARTICLE INFO

### Keywords:

Cyclic deformation  
FCC metallic materials  
Mesoscale dislocation substructures  
Single crystal

## ABSTRACT

Cyclic deformation of metallic materials depends on the interaction of multiple mechanisms across different length scales. Solid solution atoms, vacancies, grain boundaries, and forest dislocations interfere with dislocation glide and increase the macroscopic strength. In single phase metallic materials under cyclic loading, the localization of dislocation densities in sessile substructures explains a significant fraction of the strain hardening. Upon cycling, these dislocation structures evolve across stable configurations, which depend on the strain accumulation.

This work advances substructure-sensitive crystal plasticity models capable of quantifying the cyclic hardening history at various temperatures for single phase FCC materials. The framework predicts the cyclic evolution of dislocation substructure based on the activation of cross slip for Al, Cu, and Ni single- and poly-crystals up to 0.5 homologous temperature. The increase in cross slip with temperature and deformation induces a transformation in dislocation structures, which predicts secondary hardening without any additional provision. Moreover, the approach relies on material-invariant mesoscale parameters that are specific to dislocation substructures rather than a material system. Hence, we demonstrate that crystal plasticity predictive power can be augmented by parameterizing the model with single crystal experimental data from multiple materials with common substructures. As a result, the crystal plasticity model shares parameter information across materials without the need for additional single crystal experimental data for calibration.

## 1. Introduction

Numerous crystal plasticity approaches have been proposed (Roters et al., 2010) to predict the macroscopic response of metals and alloys, but most models lack predictive power at the local scale (Pokharel et al., 2014; Sangid, 2019). Researches have traditionally mitigated modeling error by proposing novel physics-based formulations that often lack rigorous assessments of model input errors (Roy and Oberkamp, 2011). In reality, limited experimental data makes it difficult (or impossible) to identify independently a large number of parameters in crystal plasticity. The lack of parameter uniqueness is ubiquitous in crystal plasticity and researchers (El Shawish and Cizelj, 2017; Pirgazi and Kestens, 2021) have demonstrated that models with different parameters do not agree on the grain scale response. As a result, damage prognosis at the grain scale still suffers from low predictive power (Pokharel et al., 2014; Sangid, 2019) and affects fatigue crack variability predictions (Rovinelli et al., 2017; Ashraf et al., 2022).

Parameter identification approaches based on mathematical fitting to macroscopic stress-strain curves (Sedighiani et al., 2022;

<sup>\*</sup> Corresponding author.

E-mail address: [castellg@cranfield.ac.uk](mailto:castellg@cranfield.ac.uk) (G.M. Castelluccio).

<https://doi.org/10.1016/j.ijplas.2022.103494>

Received 8 August 2022; Received in revised form 26 November 2022;

Available online 5 December 2022

0749-6419/© 2022 The Author(s).

Published by Elsevier Ltd.

This is an open access article under the CC BY license

(<http://creativecommons.org/licenses/by/4.0/>).

Herrera-Solaz et al., 2014), including artificial intelligence, are also ineffective since they explore shallow objective functions with multiple local minima. Different sets of parameters with marginal differences in their objective functions can result in widely different mechanical responses. Hence, optimization tools do not address the lack of experimental data that hinders independent parameter identification. Instead, the solution to independent parameterizations lies on data fusion across scales (Sangid, 2019).

Multiple researchers (Estrin et al., 1996; Estrin et al., 1998; Sedláček and Blum, 2002; Brahme et al., 2011; Steckmeyer et al., 2012; Sauzay et al., 2014) explored mesoscale data augmentation by informing strain hardening models with the morphology of sessile dislocation substructures. These approaches enable additional validation by parameterizing the response of substructures characterized with transmission electron microscopy (TEM). Castelluccio and McDowell (Castelluccio and McDowell, 2017) further extended these efforts and proposed a substructure-sensitive cyclic crystal plasticity parameterized for Ni under saturated cyclic conditions (i.e., the cyclic stress-strain loop and dislocation structures do not change upon further cycling). This model incorporates length scales and evolution laws associated with mesoscale dislocation substructures that were validated with single- and poly-crystal experimental data. The approach successfully predicted the saturated cyclic response single- and poly-crystal by relying the similitude principle (Sauzay and Kubin, 2011), in which the structure spacing ( $d_{struct}$ ) is inversely related to the maximum shear stress ( $\tau_{max}$ ),

$$d_{struct} = K_{struct} \frac{\mu b}{\tau_{max}}. \quad (1)$$

Here,  $b$  is the Burgers vector,  $\mu$  is the shear modulus, and  $K_{struct}$  is the similitude coefficient, which does not significantly depend on temperature or the material (Nakanishi et al., 2013; Sauzay and Kubin, 2011). Thus, predicting the correct structure spacing is akin to validating the local shear stress. Also, validation with single crystals—uncommon on the crystal plasticity literature—supports the comparison with lower scale discrete approaches (e.g., dislocation dynamics), which are not large enough to encompass polycrystals.

More recently, Dindarlou and Castelluccio (Dindarlou and Castelluccio, 2022) developed a substructure-sensitive crystal plasticity approach for monotonic loading and demonstrated that identical ‘material-invariant’ mesoscale parameterizations can predict the response of Ni, Cu, and Al single- and poly-crystals. This work demonstrated that fitting models only to polycrystalline stress-strain curves underpredicts intergranular variability. In addition, the approach mitigated model input errors by demonstrating that parameters associated with strain hardening from sessile dislocation structures can be calibrated using single crystal data from proxy materials.

The notion of mesoscale material-invariance attributes is supported by the experimental findings from Li and coworkers (Li et al., 2011), who reviewed the commonalities among cyclic deformation dislocation substructures in FCC metals and their effect on the macroscopic stress-strain responses. Their work demonstrated that cyclic loading of different FCC metallic materials (Ni, Cu, and Ag) evolve similar dislocation substructures: veins, PSBs, cell, and labyrinth. This taxonomy of substructures applies to other materials such as stainless steel (Pham et al., 2013), high entropy alloys (Picak et al., 2021), and Al (Charsley et al., 1989; M Videm and Ryum, 1996). In particular, Al single crystals oriented for single slip at 77 K develop vein structures (Kassner et al., 1997) that transform into PSBs (Nakanishi et al., 2013), which are similar to those found in Ni (Holzwarth and Essmann, 1993) and Cu (Basinski et al., 1980; Tippelt et al., 1997) at room temperature. However, Al forms cells rather than PSBs at room temperature (Vorren and Ryum, 1988; Vorren and Ryum, 1987; Giese and Estrin, 1993), which lead some researchers (Grosskreutz and Mughrabi, 1975) to believe that Al resulted in the *high-strain-amplitude* structures found Cu and Ni. These results suggests that the cyclic crystal plasticity proposed by Castelluccio and McDowell (Castelluccio and McDowell, 2017) can be extended to consider various FCC materials at different temperatures as long as they develop similar mesoscale parameters.

Experimental efforts (Mughrabi, 1978) have also shown that the cyclic history is strongly linked to the dominant dislocation substructures and their stability. Low cycle fatigue of Cu at room temperature results in a stable mechanical response and unchanging dislocation structures after a few hundred cycles (Rie, 1987). In the very high cycle regime, stress saturation typically takes tens to hundreds of thousands of cycles (Polak et al., 1988). Other studies (Wang and Mughrabi, 1984) showed that Cu crystals oriented for single slip at room temperature do not saturate but develop secondary hardening; a similar phenomenon is observed for Cu at 523 K (Lisiecki and Weertman, 1990) at lower number of cycles. Thus, modeling approaches above 0.2 of the homologous temperatures, large strains, or for very large number of loading cycles cannot assume the saturation of the stress-strain loop as proposed by Castelluccio and McDowell (Castelluccio and McDowell, 2017).

TEM characterization of Al, Cu, and Ni (Lisiecki and Weertman, 1990; Fougères, 1993; Bretschneider et al., 1997) further demonstrated that secondary hardening occurs due to the transformation of PSBs into cells (provided cracking is avoided). Cell formation mechanisms are not entirely understood, but cross slip is often observed to be a necessary requirement (Obertlík et al., 1994; Mitchell and Teer, 1970). Hence, the transition from PSBs to cells requires the activation of cross slip through cyclic hardening or higher temperatures. For example, early PSB structures in Al single crystals at room temperature (Dhers and Driver, 1988) soon evolve into cells and secondary hardening upon further cycling. These experimental results corresponds to homologous temperatures about 0.35, roughly equivalent to that corresponding to 523 K for Cu (Lisiecki and Weertman, 1990). Hence, modeling changes to substructures could account for cyclic history across at different temperatures. In addition, the commonalities among materials substructures suggests that material-invariant parameterization demonstrate for monotonic loading (Dindarlou and Castelluccio, 2022) could also be found for cyclic deformation.

This work extends substructure-sensitive approaches to predict primary and secondary cyclic hardening in single-phase FCC materials at various temperatures for which no saturation is achieved. We make use of Al single- and poly-crystal data to parameterize mesoscale substructures and we demonstrate that the same mesoscale parameters predict the cyclic response of Ni and Cu. We further propose the notion that the accumulation of cross slip activity can serve as an indicator for the transition of PSBs into cells structures, which can be triggered by high temperatures or large deformations. The results demonstrate a robust modeling approach to quantify

initial and secondary hardening induced by deformation or temperatures. Our analysis further demonstrates that mesoscale parameters for cyclic loading are material-invariant and they are intrinsically related to structures.

## 2. Substructure-sensitive crystal plasticity modeling

The basis of the substructure-sensitive crystal plasticity models were proposed by Castelluccio (Castelluccio and McDowell, 2017; Dindarlou and Castelluccio, 2022) and assumed that the plastic shear rate along  $\alpha^{th}$  slip system follows the thermally-activated flow rule (Kocks et al., 1975),

$$\dot{\gamma}^\alpha = \dot{\gamma}_0^\alpha \exp \left[ -\frac{F_0}{k_B T} \left\langle 1 - \left[ \frac{\langle |\tau^\alpha - B^\alpha| - S^\alpha \rangle}{s_0^\alpha \frac{\mu}{\mu_0}} \right]^p \right\rangle^q \right] \text{sgn}(\tau^\alpha - B^\alpha), \quad (2)$$

where,  $\dot{\gamma}_0^\alpha$  is the effective shearing rate,  $k_B$  is the Boltzmann constant,  $F_0$  is the glide activation energy,  $s_0^\alpha$  is the thermal stress at 0 K, and  $p$  and  $q$  are the profile parameters. Also,  $\mu_0$  is the shear modulus at 0 K. Additionally,  $\langle G \rangle = 0$  if  $G \leq 0$  or  $\langle G \rangle = G$  if  $G > 0$ . For continuous flow, dislocations must overcome the effective shear stress ( $\tau_{eff}^\alpha$ ) with the aid of thermal activation,

$$\tau_{eff}^\alpha = |\tau^\alpha - B^\alpha| - S^\alpha, \quad (3)$$

which corresponds to the local resolved shear stress ( $\tau^\alpha$ ) less the strengthening from the athermal stress ( $S^\alpha$ ) and intragranular back stress ( $B^\alpha$ ). We further assume that the athermal stress follows the relation,

$$S^\alpha = \alpha_{LE} \frac{\mu b}{2d_{struc}} + \mu b \sqrt{A_{ii} \rho^\alpha}, \quad (4)$$

in which the first term represents the stress required to bow-out dislocations a distance  $d_{struc}$  and controls dislocation production. The second term corresponds to the dislocation self-interaction strength and controls coplanar hardening through the balance of mobile dislocation densities ( $\rho^\alpha$ ). In Eq. (4),  $\alpha_{LE}$  is the dislocation line energy coefficient and  $A_{ii}$  is the self-interaction coefficient. Note that experimental evidence (Sauzay and Kubin, 2011; Kocks et al., 1975) has suggested that parameters in Eq. (4) are approximately temperature independent. We further consider an intragranular back stress (Castelluccio and McDowell, 2017) that represents the constraint imposed on mobile dislocations by sessile dislocation structures,

$$B^\alpha = \frac{f_w}{1 - f_w} \frac{2\mu(1 - 2S_{1212})}{1 + 4S_{1212}\mu f_{Hill}^S} \dot{\gamma}^\alpha, \quad (5)$$

where,  $f_w$  is the wall volume fraction,  $f_{Hill}^S$  is the instantaneous macroscopic plastic deformation tangent,

$$f_{Hill}^S = \frac{1}{2} \frac{d\gamma^\alpha}{d\tau}. \quad (6)$$

The Eshelby tensor component ( $S_{1212}$ ) for a prolate spheroid coordinate system follows (Mura and Ting, 1989),

$$S_{1212} = \frac{\pi\eta^2 + (\eta^2 - 1.75 - 2\nu_p\eta^2 + 2\nu_p)C_{12}}{8\pi(1 - \nu_p)(\eta^2 - 1)}, \quad (7)$$

$$C_{12} = \frac{2\pi\eta(\eta\sqrt{(\eta^2 - 1)} - \cosh^{-1}\eta)}{\sqrt[3]{(\eta^2 - 1)}}, \quad (8)$$

and,

$$\nu_p = \frac{\nu + \frac{2}{3}\mu(1 + \nu)f_{Hill}^S}{1 + \frac{4}{3}\mu(1 + \nu)f_{Hill}^S}. \quad (9)$$

Here,  $\nu_p$  is the tangent elasto-plastic Poisson's ratio, and  $\nu$  is the elastic Poisson's ratio. The dislocation mean free path along the dominant slip plane ( $l_{struc}$ ) is often computed proportionally to the square root of the dislocation densities (Wang et al., 2017; Sedighiani et al., 2020), i.e.,

$$l_{struc} = \alpha' \mu b \frac{1}{\sqrt{\rho^\alpha}}. \quad (10)$$

However, a constant  $\alpha'$  for all crystal orientation under predicts intrinsic glide heterogeneity (Dindarlou and Castelluccio, 2022; Devincere et al., 2008). Instead, we consider the analysis by Sauzay and Kubin (Sauzay and Kubin, 2011), who demonstrated that  $d_{struc} \propto \frac{1}{\sqrt{\rho^\alpha}}$ . Following this relation and Eq. (10) we proposed (Castelluccio and McDowell, 2017),

$$l_{struc} = \eta d_{struc} \quad (11)$$

in which  $\eta$  corresponds to the anisotropic aspect ratio of each dislocation structures. We further limit the mean glide distance of dislocations to a fraction of the  $d_{grain}$  to account for grain boundary obstacles, i.e.,

$$\text{If } l_{struc} > 0.25d_{grain} \text{ then } l_{struc} = 0.25d_{grain} \tag{12}$$

This limit to the mean free path assumes that crystals that are tens to hundreds microns in size for which plasticity is driven by the bulk of the grain rather than the grain boundary. Hence, a dislocation can glide only a fraction of the grain size before they encounter a grain boundary (ignoring the cases in which they can cross it). This strategy provides a simple and physically sensible strategy to introduce the grain/crystal size length scale in crystal plasticity.

Finally, the effective shearing rate depends on the jump frequency over point obstacles ( $v_G$ ),

$$\dot{\gamma}_0^\alpha = \rho^\alpha b l_{struc} v_G, \tag{13}$$

and the total mobile dislocation density is computed as the net result of dislocation multiplication, annihilation, and cross slip. (Castelluccio and McDowell, 2017),

$$\begin{aligned} \dot{\rho}_m^{\alpha\alpha} = & \frac{k_{multi}}{bl_{struc}} |\dot{\gamma}^\alpha| - \frac{2y_s^{edge}}{b} \rho_m^{\alpha\alpha} |\dot{\gamma}^\alpha| - \frac{2\pi}{\mu b d_{struc}} |\dot{\tau}_{eff}| |^{unload} \\ & + v_G \frac{d_{struc}}{d_0} \left( \phi_{cs} \sum_{\xi=1}^N \rho_m^{\alpha\xi} e^{\left( -V_{CS}^\alpha \frac{\mu b}{4\pi y_s^{screw}} \frac{|\tau^\alpha - B^\alpha|}{k_B T} \right)} - (1-\phi) \sum_{\xi=1}^N \rho_m^{\alpha\xi} e^{\left( -V_{CS}^\alpha \frac{\mu b}{4\pi y_s^{screw}} \frac{|\tau^\alpha - B^\alpha|}{k_B T} \right)} \right), \end{aligned} \tag{14}$$

Here,  $k_{multi}$  determines the number of dislocations produced per plastic strain increment and  $y_s^{edge}$  and  $y_s^{screw}$  are the annihilation distances for edge and screw dislocations respectively. Also,  $V_{CS}^0 = 1000b^3$  corresponds to the cross-slip activation volume and  $\phi = 0.5$  is the cross-slip efficiency that represents the likelihood of annihilation from cross slipping. Finally, we assume for well annealed materials an initial mobile dislocation density of  $10^9 m^{-2}$  and an initial structure spacing of  $10 \mu m$  with  $\eta = \eta_{veins}$  and  $f_w = 0.1$ .

### 2.1. Mesoscale substructure identification

Early efforts by Castelluccio and McDowell (Castelluccio and McDowell, 2017) parameterized the morphology of dislocation structures ( $f_w$  and  $\eta$ ) assuming saturated structures after thousands of loading cycles. Here, we avoid this limitation by proposing that mesoscale parameters depend on a pre-assumed number of loading cycles ( $N$ ). Hence, we define  $N$  as an input with the understanding that the model describes the cyclic response expected after  $N + 1$  cycles.

Fig. 1 presents a novel scheme to identify the dominant dislocation structure after  $N$  cycles for each material point. This approach

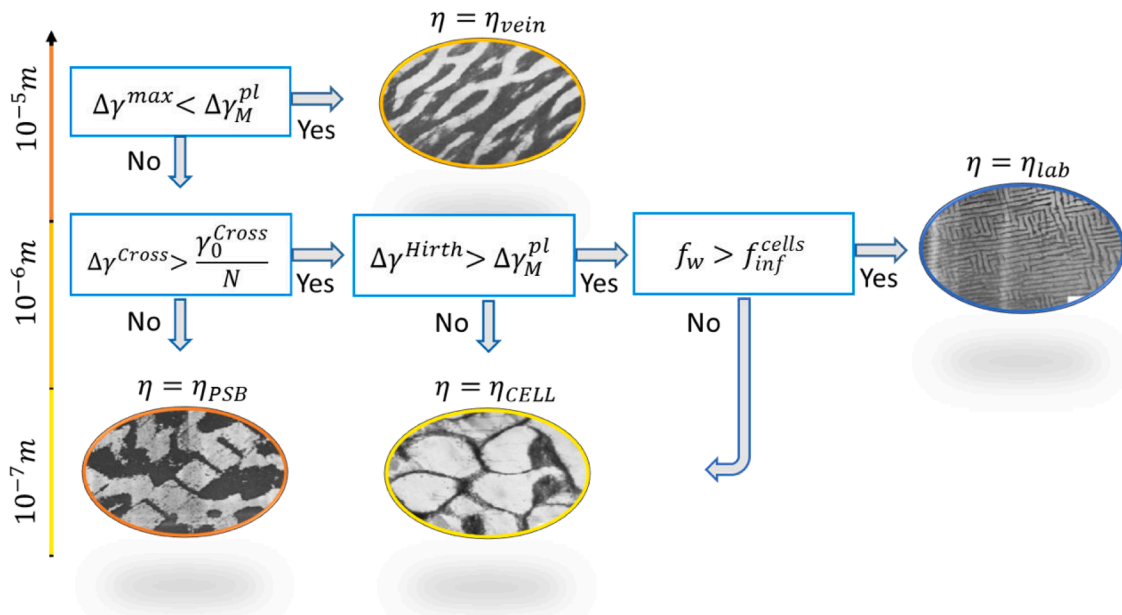


Fig. 1. Framework for assigning saturated dislocation substructure at each FE integration point depending on  $\Delta\gamma_p$  among slip systems that are a function of different loading conditions applied at a time.

relies on comparing the partition of plastic shear range per cycle ( $\Delta\gamma^{\alpha}$ ) among different slip systems ( $\alpha$ ). Here,  $\Delta\gamma^{max}$  corresponds to the maximum cyclic plastic shear range and has one slip plane associate to cross-slip, whose plastic shear range we refer to as  $\Delta\gamma^{cross}$ . Similarly, the  $\Delta\gamma^{max}$  slip plane has two slip systems associated to Hirth locks, and their corresponding plastic shear ranges are referred to as  $\Delta\gamma^{Hirth}$ .

We propose that veins evolve into more stable structures if  $\Delta\gamma^{max}$  is larger than the matrix threshold  $\Delta\gamma_M^{pl}$ , which has a typical value in the range of  $\Delta\gamma_M^{pl} \approx 5 \times 10^{-5}$  to  $1 \times 10^{-4}$  (Mughrabi, 1978; Bretschneider et al., 1997; Dhers and Driver, 1988). We also propose that the transformation of PSBs into cells occurs when the cumulative plastic shear strain in cross slip planes ( $\gamma_{cum}^{Cross}$ ) surpasses a critical threshold  $\gamma_0^{Cross} \approx 0.08$  for Al. The quantification of  $\gamma_{cum}^{Cross}$  would require explicitly modeling of every loading cycle up to  $N$ , which can be computationally burdensome. Instead, we consider the shear range on the cross-slip plane ( $\Delta\gamma^{Cross}$ ) and approximate the accumulation of plasticity as follows,

$$\gamma_{cum}^{Cross} = N \Delta\gamma^{Cross}, \tag{15}$$

and we predict that the transition into cells occurs when,

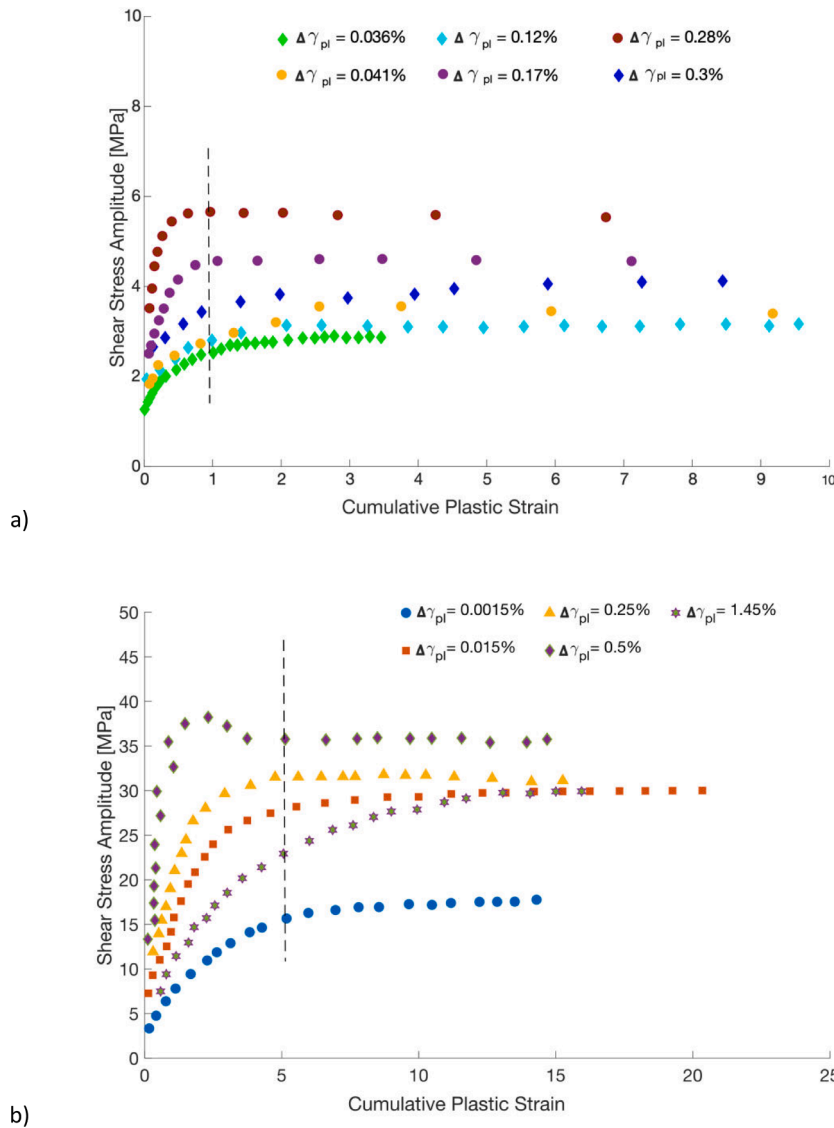


**Fig. 2.** Experimental cyclic shear stress as a function of cumulative plastic strain for a) Al (Vorren and Ryum, 1987; Alhamany et al., 1992) b) Cu (Mughrabi, 1978), for various applied plastic shear strain ranges. Stress saturates upon reaching a critical cumulative plastic strain of  $\gamma_{pl}^* \approx 1$  for Al (Vorren and Ryum, 1987; Alhamany et al., 1992) and  $\gamma_{pl}^* \approx 5$  for Cu (Mughrabi, 1978; Lisiecki and Weertman, 1990; Alhamany et al., 1992). Note that these values do not depend on the applied plastic shear strain range.

$$\Delta\gamma^{Cross} > \frac{\gamma_0^{Cross}}{N}. \tag{16}$$

Because cross slip increases with temperature and deformation, this approach can also describe the transition into cells at high temperatures and applied deformation without any additional provision.

Under cyclic deformation, the wall fraction is computed with a modified approach from that proposed by Castelluccio et al. (Castelluccio and McDowell, 2017), which was based on the work by Estrin et al. (Estrin et al., 1998),

$$f_w = f_{inf} + (f_{oi} - f_{inf}) \exp\left(\frac{-\Delta\gamma^{max}/2}{g_p}\right). \tag{17}$$

Here,  $f_{oi}$  is a transient wall volume fraction that depends on  $N$  and  $f_{inf}$  is the intrinsic wall fraction of a structure (e.g., when a single structure that occupies the entire crystal volume, typically at larger strains). Also,  $g_p$  is a parameter that regulates the rate of decrease of  $f_w$  with strain rate and equals to  $1.5 \times 10^{-3}$ .

Cyclic experiments for Al and Cu (Mughrabi, 1978; Bretschneider et al., 1997; Alhamany et al., 1992) have shown that the stress saturates at a critical cumulative plastic strain ( $\gamma_{pl}^*$ ), which depends on the material but not on the applied plastic shear strain range. Fig. 2(a) suggests that in Al, an accumulated plastic shear strain about 0.5 to 1.5 triggers the transition of structure after a few hundred cycles.

We argue that the critical cumulative plastic strain to achieve stress saturation is the manifestation of the a stable dislocation wall fraction. Hence, we propose to describe transients up to saturation with an increasing wall fraction that depends on  $N$ , and the intrinsic the volume fraction of veins substructures,  $f_{veins}$ , (Suresh, 1998; Hecker et al., 1997),

$$\left. \begin{aligned} f_{oi} &= f_{veins} \times \left(\frac{N \times \Delta\gamma^{max}}{\Delta\gamma_{pl}^*}\right) \text{ if } \frac{N \times \Delta\gamma^{max}}{\Delta\gamma_{pl}^*} \leq 1 \\ f_{oi} &= f_{veins} \text{ if } \frac{N \times \Delta\gamma^{max}}{\Delta\gamma_{pl}^*} > 1 \end{aligned} \right\} \tag{18}$$

Here, the  $\Delta\gamma^{max}$  is the range of cyclic plastic strain in the most active slip system and  $\Delta\gamma_{pl}^* \approx 1$  for Al (Vorren and Ryum, 1987; Alhamany et al., 1992) and  $\Delta\gamma_{pl}^* \approx 5$  for Cu (Mughrabi, 1978; Lisecki and Weertman, 1990; Alhamany et al., 1992). In the case  $f_{oi}$  is less than  $f_{veins}$ ,  $f_w$  corresponds to the volume fraction of initial hardening stage following Eq. (18). Once  $f_{oi}$  reaches  $f_{veins}$ , the maximum accumulation of veins has been attained and they will start transforming into a more stable structure. Fig. 3 presents the wall fraction computed by combining Eqs. (17) and ((18). At low number of cycles, the wall fraction increases monotonically with increasing plastic shear strains, as it is the case for tensile loading (Dindarlou and Castelluccio, 2022). At a high number of cycles, which corresponds to stress saturation shown as a red line, the wall fraction decreases with increasing plastic shear strain, as assumed by Estrin et al. (Estrin et al., 1998) and Castelluccio and McDowell (Castelluccio and McDowell, 2017).

### 2.2. Independent estimation of parameters for Al

Parameters related to atomic unit processes, such as elastic constants are strongly dependent on the composition. For Al, the Burgers vector is taken to be  $b = 0.286$  nm (Kocks et al., 1975) and the elastic constants depend on temperature (Varshni, 1970),

$$C_{11} = 10^5 \left(1.142 - \frac{0.10111}{\exp\left(\frac{2539.4}{T}\right) - 1}\right),$$

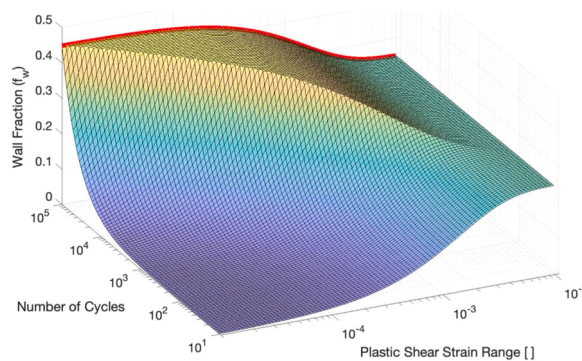


Fig. 3. Calculation of the wall fraction combining Eqs. (17) and (18). Depending on the number of cycles applied, the wall fraction increases or decreases for higher applied plastic strain ranges. The red line corresponds to the saturated state previously assumed by Castelluccio and McDowell (Castelluccio and McDowell, 2017).



$$C_{12} = 10^5 \left( 0.6195 - \frac{0.0205109}{\exp\left(\frac{293.6}{T}\right) - 1} \right), \quad (19)$$

$$C_{44} = 10^5 \left( 0.3160 - \frac{0.0256479}{\exp\left(\frac{148.8}{T}\right) - 1} \right),$$

$$\mu = 29156 \text{ MPa} \frac{C_{44}(T)}{C_{44}(0K)}.$$

The glide activation energy ( $F_0$ ), thermal stress ( $s_0^t$ ), and profiling parameters  $p$  and  $q$  are taken as atomic unit processes that depend on the material and can be estimated independently using yield stress data as a function of temperature (Ashraf and Castelluccio, 2021). The jump attempt frequency is estimated as  $\nu_G = 5 \times 10^{11} \text{ s}^{-1}$  (Langer et al., 2010), while the annihilation distances for edge ( $y_e$ ) and screw ( $y_s$ ) dislocations in Eq. (14) were also estimated independently for Al, Ni and Cu from experimental data (Basinski et al., 1980; Tippelt et al., 1997; Kassner and Wall, 1999; Feugas, 1999; Essmann and Mughrabi, 1979). Table 1 summarizes the atomic unit process parameters on the crystal plasticity model for Al.

Mesoscale parameters include the aspect ratio of each substructure ( $\eta_i$ ), dislocation self-interaction coefficient ( $A_{ii}$ ), similitude coefficient ( $K_{struc}$ ), and line-energy coefficient ( $\alpha_{LE}$ ), which are less sensitive to the composition. Table 2 presents the best estimates for these parameters for Al, which were computed independently using experimental and bottom-up modeling approaches (Nakanishi et al., 2013; Sauzay and Kubin, 2011; Devincere et al., 2008; Kubin et al., 2008; Fivel et al., 1998; Schwartz et al., 2013; Madec et al., 2003; Hachet et al., 2020; Szajewski et al., 2015; Tabata et al., 1982; Armstrong and Rodriguez, 2006; Tabata et al., 1978).

Following the analysis of TEM images at various temperatures and materials (Ashraf and Castelluccio, 2021), we computed the volume fraction at saturation as the ratio between the wall thickness and wall spacing (Oudriss and Feugas, 2016). This analysis demonstrated that veins and cells have a constant wall fraction independent of temperature ( $f_{veins} \approx 0.45$  and  $f_{inf}^{cells} \approx 0.22$ ). On the contrary, Fig. 4 demonstrates that the volume fraction of PSBs ( $f_{inf}^{PSB}$ ) decreases with increasing temperature while the volume wall fraction for labyrinth structures ( $f_{inf}^{Lab}$ ) are also temperature dependent and proportional to  $\frac{1}{\sqrt{2}} f_{inf}^{PSB}$  (Ashraf and Castelluccio, 2021). Table 3 presents the values employed for  $f_{inf}^{PSB}$  in Al simulations at 77 K and 293 K (0.083 and 0.32 homologous temperature, respectively).

### 2.3. Model implementation

The framework was implemented using Abaqus UMAT and UEXTERNALDB subroutines (ABAQUS 2017) along with a regular mesh made of brick elements (C3D8R). Four single crystal orientations—[123, 011, 001], and [111]—are considered using meshes with 500 elements. Polycrystal models use 5000 brick elements and 122 grains with average grain size of 80  $\mu\text{m}$  as shown in Fig. 5. The microstructure was recreated with Dream3D (Groeber and DREAM, 2014) and an in-house Matlab script that resulted in equiaxed randomly oriented grains. This model approximates a representative volume element (RVE) of the constitutive response (which requires a much lower number of grains as compared to the RVE for fatigue evaluation (Castelluccio and McDowell, 2015)).

The simulation applies a displacement along the X-axis. Unidirectional periodic boundary conditions are specified along the x-axis and the remaining four faces of the model are left as a traction free surface in all simulations. All simulations are performed under fully reversed ( $R_\epsilon = -1$ ) quasistatic deformation at a rate of  $10^{-4}$ , which approximate the experimental testing conditions.

## 3. Modelling results for Al

Initially, we performed simulations applying different deformation levels to compute the saturated cyclic stress-strain curve (CSSC) under fully reversed straining. Each data point in the CSSC corresponds to the peak stress range computed after 13 full computational reversals, which is sufficient to saturate the response (Ashraf et al., 2022). Fig. 6(a) compares experimental and modeling results for Al single crystals at 298 K, deformed along [001] and [123] directions at a strain rate of  $1 \times 10^{-3} \text{ s}^{-1}$ . Experiments (Videm and Ryum, 1996) showed that [001] crystals results in stable CSSCs after a few thousand cycles. On the contrary, Dhers and Driver (1988) showed that [123] crystals reach different stress levels after 100 cycles or upon reaching  $\gamma_{cum}^{pl} = 50$ .

Our simulation results in Fig. 6(a) indeed capture the saturation of the CSSC for [001] crystals, for which the stress stabilizes after thousands of cycles (shown in Fig. 7). In the case of crystals oriented for single slip, we computed the CSSC by predefining  $N$  such that  $\gamma_{cum} = 4N\Delta\gamma_{pl}$  (Suresh, 1998) ( $\Delta\gamma_{pl}$  being the plastic shear strain amplitude). The model reproduces the secondary hardening that

**Table 1**

Atomist unite process parameters for Al estimated using yield stress data (Ashraf and Castelluccio, 2021) and observed in experiments (Basinski et al., 1980; Tippelt et al., 1997; Kassner and Wall, 1999; Feugas, 1999; Essmann and Mughrabi, 1979).

Material	$F_0$ (eV)	$s_0^t$ (MPa)	p	q	$y_s$ (nm)	$y_e$ (nm)
Al	0.8	12	0.667	1.5	50	3.5

**Table 2**  
Al mesoscale parameters related to long range interactions.

	$\eta_{PSB}$	$\eta_{lab}$	$\eta_{cells}$	$\xi_p$	$K_{multi}^{walls}$	$K_{multi}^{cell}$	$A_{ii}$	$\alpha_{LE}$	$G_M$	$K_{struc}$
50	20	5	1	0.0015	2	1	0.1	1	$10^{-4}$	2.5

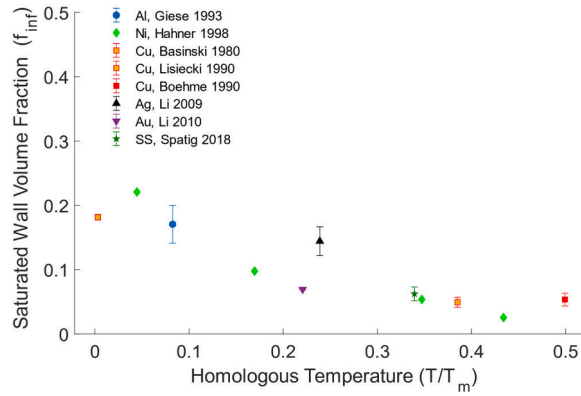


**Fig. 4.** Saturated wall volume fraction of PSB as a function of homologous temperature for different FCC metals (Basinski et al., 1980; Giese and Estrin, 1993; Lisiecki and Weertman, 1990; Hähner et al., 1998; Boehme et al., 1990; Li et al., 2009; Spätig et al., 2018; Li et al., 2010).

**Table 3**  
Temperature dependent wall fraction for PSBs and labyrinth structures in Al.

Homologous temperature	0.083	0.32
$f_{inf}^{PSB}$	0.29	0.1
$f_{inf}^{lab}$	0.21	0.07

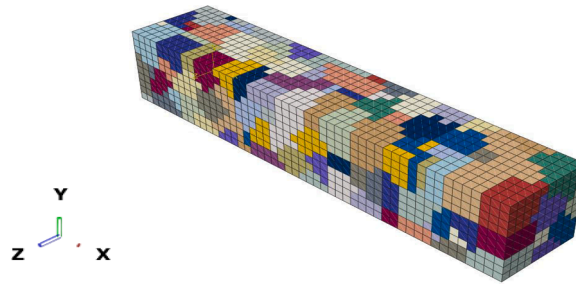


**Fig. 5.** Finite element mesh of a polycrystal specimen containing 5000 elements and 250 grains. Colors represent different grains.

occurs upon further cycling at high plastic strains without any special provision. Notably, the model also predicts the lack of secondary hardening at low strains thanks to the stability of PSBs and the limited availability of cross slip.

Next, Fig. 6(b) presents the CSSC for Al single crystals oriented for single slip and deformed at 77 K, which experiments have shown to be stable even at high strains (Nakanishi et al., 2013). The model correctly predicts the cyclic stress level of the plateau and no additional hardening with cycling at 77 K (also shown in Fig. 7). We highlight that the model successfully describes the CSSC at saturation, or the lack of it, for Al crystals by introducing only a temperature dependence for  $f_{inf}^{PSB}$ .

Fig. 7 further compares the cyclic history of Al single crystals from models and experiments. Single crystals deformed at 293 K along [123] direction with different cyclic strains result in initial cyclic hardening from veins bundles until reaching a volume fraction close to 50%. At that point, veins coexist with PSBs until cross slips enables the transition into cells, which results in additional hardening as suggested by Lisiecki and Weertman (Lisiecki and Weertman, 1990). Fig. 7 also present the modeling results for [001] crystals at 293 K or [123] crystals at 77k, for which no experimental data is available. In both cases, stress saturation occurs at lower number of cycles without evidence of secondary hardening. Finally, Fig. 7 presents the results (diamond symbol) from updating N every cycle, which represents the cycle-by-cycle response. Given the computational cost, we present only 100 cycles using initial dislocation density of  $10^{11}m^{-2}$ . Hence, we demonstrate that explicitly applying hundreds of cycles is equivalent to our accelerated approach in which we



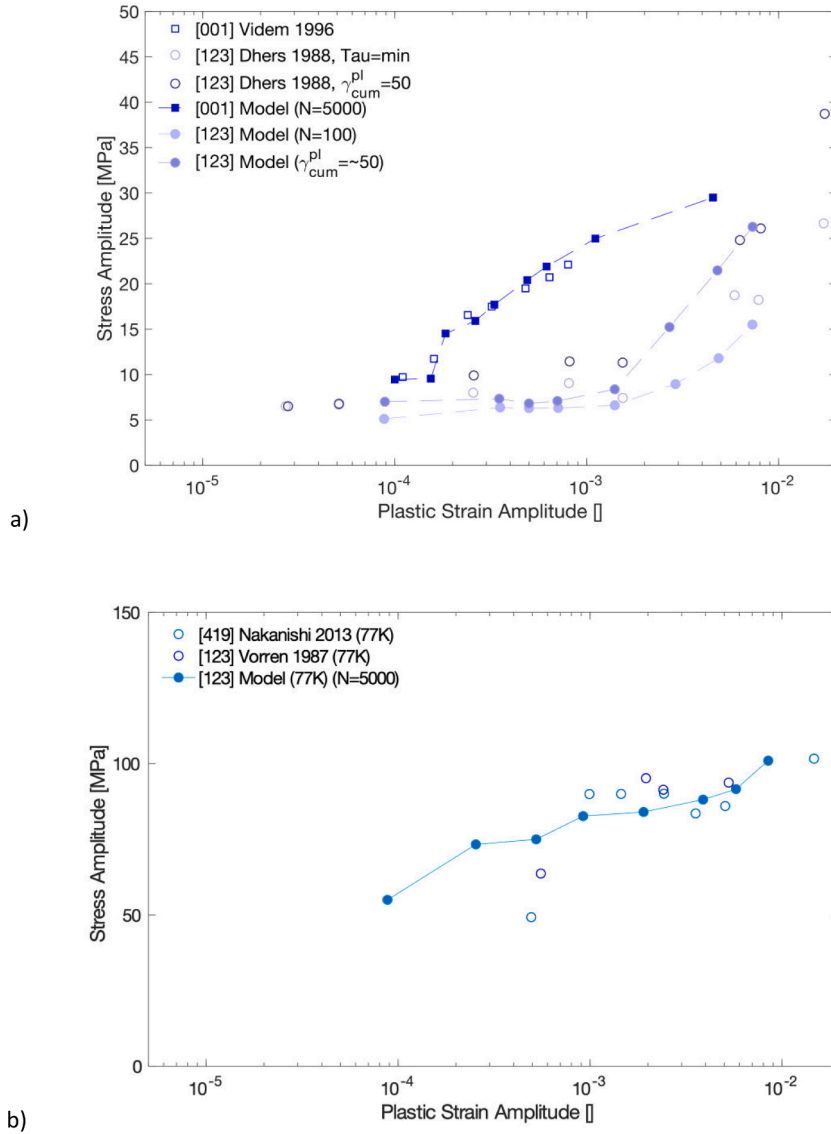


**Fig. 6.** Fully reversed cyclic stress-strain response of Al single crystals deformed along a) [001] and [123] at 298 K and b) [123] at 77 K. Both [001] (298 K) and [123] (77 K) crystals reach saturation and the modeled assuming  $N = 5000$ . The [123] crystals at 298 K show different stress levels at  $N = 100$  or  $\gamma_{cum}^{pl} = 50$ . The results are compared with experiments from (M Videm and Ryum, 1996; Dhers and Driver, 1988; Wang et al., 1999) at 298 K and from (Nakanishi et al., 2013; Vorren and Ryum, 1987) at 77 K.

predict the response for  $N + 1$  cycle.

Since the model identifies the dominant dislocation structure at each finite element (Fig. 1), we can quantify the total volume fraction occupied by each structure. Fig. 8 presents the volume fraction occupied by PSBs and cells as a function of plastic strain range and demonstrates how cells dominate at high plastic strains. At low strains, limited cross slip prevents from the accumulated cross slip range to surpasses the critical magnitude  $\frac{\gamma_0^{cross}}{N}$  introduced in Fig. 1.

A central advantage of substructure-sensitive models is their ability to validate mesoscale attributes from TEM microscopy. We further inspected dislocation structures from experiments at various temperatures (Nakanishi et al., 2013; M Videm and Ryum, 1996; Fujii et al., 2008) and measured their wall spacing. These results along with the model predictions are compared in Fig. 9, which further demonstrates that the substructure-sensitive model captures the macroscopic and mesoscopic responses.

Since dislocation structures are identified by surveying the partition of plastic deformation, not crystal orientation, we next apply the model to polycrystalline materials without any recalibration. We note that grain size effects are conveyed by Eq. (12), which should be valid for grains at least tens of microns in size (i.e., no grain-boundary-controlled plasticity or dislocation starvation). Fig. 10 compares the CSSC for Al polycrystals from experiments and simulations at  $N = 5000$  and demonstrates the model ability to predicted the stress response of the polycrystal and grain size effects. Fig. 11 further presents excellent agreement with the stabilized stress-strain

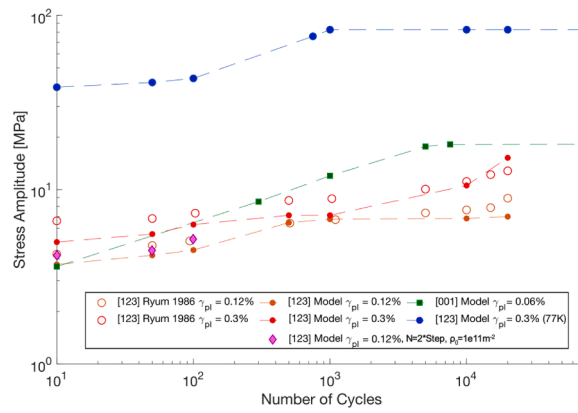


**Fig. 7.** Cyclic hardening of Al single crystal at 298 K and 77 K. Circles correspond to single slip crystals deformed at 0.12% or 0.3% plastic shear strain ranges while squares corresponds to multiple slip [001] crystal under 0.06% plastic shear strain ranges. Note the saturation of the stress after a thousand cycles for [001] crystal at room temperature and [123] at 77 K. Hollow and full symbols correspond to experiments and simulations respectively.

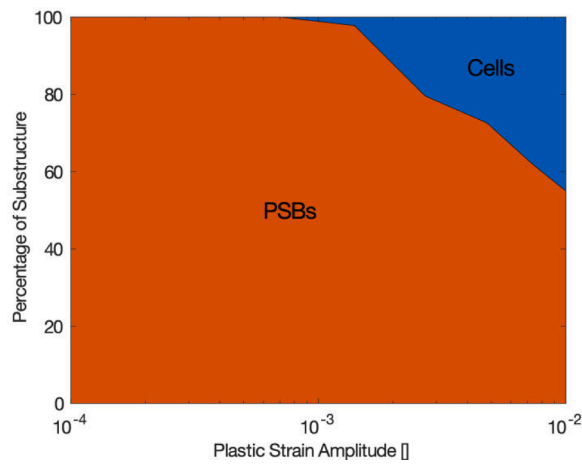


**Fig. 8.** Percentage of dominant dislocation substructure among 500 elements at  $\gamma_{cum}^{pl} = 50$  as function of plastic strain amplitude.

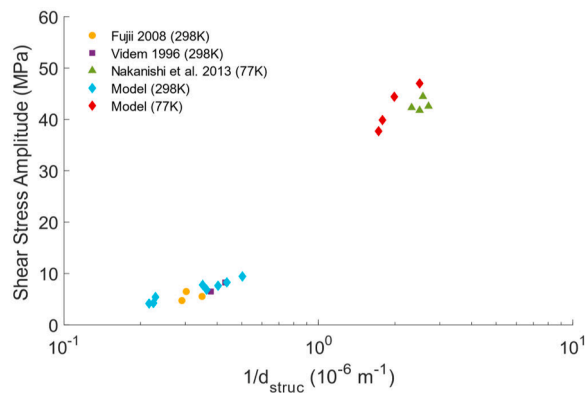


**Fig. 9.** Comparison of wall spacing measured from experiments (Nakanishi et al., 2013; M Videm and Ryum, 1996; Fujii et al., 2008) and  $d_{struc}$  from models at different temperatures.

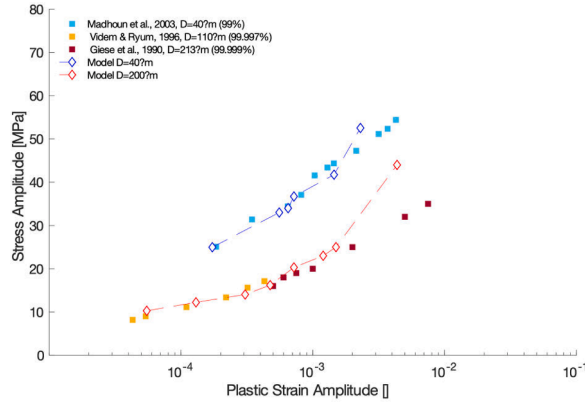


Fig. 10. Comparison between models and experiments (M Videm and Ryum, 1996; Tsou and Quesnel, 1982; Giese et al., 1990; El-Madhoun et al., 2003) of the cyclic stress-strain response of Al polycrystals with different grain sizes.

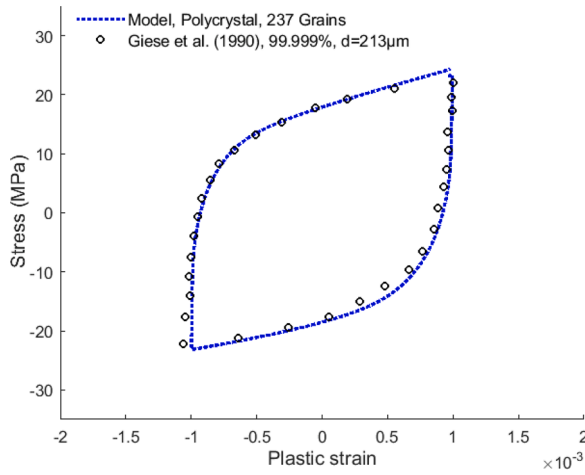


Fig. 11. Comparison of complete cyclic stress-strain response of Al polycrystal between model and experiment (Giese et al., 1990).

loop for Al polycrystal 298 K and  $\frac{\Delta \epsilon_{pl}}{2} = \sim 1 \times 10^{-3}$ .

#### 4. Mesoscale material-invariance

Castelluccio and McDowell (Castelluccio and McDowell, 2017) proposed the substructure-sensitive model to predict only the fully saturated cyclic response of Ni single- and poly- crystals at room temperature. This work extended those efforts by focusing on the entire cyclic history at different temperatures rather than just the saturation stage, which does not occur for Al at room temperature. We now explore the cyclic evolution of Ni and Cu at various temperatures, which share similar dislocation structures with Al. For these materials, the Burgers vector is taken as  $b = 0.25 \text{ nm}$  (Kocks et al., 1975) and the elastic constants depend on temperature following (Varshni, 1970),

$$C_{11} = 10^5 \left( 2.612 - \frac{0.1932}{\exp\left(\frac{310.4}{T}\right) - 1} \right),$$

$$C_{12} = 10^5 \left( 1.508 - \frac{0.05177}{\exp\left(\frac{634.1}{T}\right) - 1} \right), \tag{20}$$

$$C_{44} = 10^5 \left( 1.317 - \frac{0.07888}{\exp\left(\frac{201.1}{T}\right) - 1} \right),$$

$$\mu = 87018 \text{ MPa} \frac{C_{44}(T)}{C_{44}(0K)},$$

for Ni, and the following for Cu.

$$C_{11} = 10^4 \left( 17.6094 - \frac{0.760041}{\exp\left(\frac{206.4}{T}\right) - 1} \right)$$

$$C_{12} = 10^4 \left( 12.4892 - \frac{0.238363}{\exp\left(\frac{158.4}{T}\right) - 1} \right) \tag{21}$$

$$C_{44} = 10^4 \left( 8.170 - \frac{0.45283}{\exp\left(\frac{163.4}{T}\right) - 1} \right)$$

$$\mu = 48301.0 \text{ MPa} \frac{C_{44}(T)}{C_{44}(0K)}$$

We further employ the atomic process unit parameters in Table 4 and temperature dependence of the PSB wall fraction presented on Table 5 and Table 6. As shown by Fig. 12, the parameterization of  $f_{inf}^{PSB}$  aligns closely to that found in experiments (Fig. 4) and is almost identical for various materials and suggest that this parameter can be approximated as material-invariant. Furthermore, as shown in Fig. 2b), the transition from PSBs into cells at 298 K in Cu is delayed compared to Al. In Cu, the transition occurs after reaching an accumulated plastic shear strain of value about five regardless of the cyclic plastic strain applied (Mughrabi, 1978; Bretschneider et al., 1995). Hence, we assume that  $\gamma_{pt}^* = 5$  and  $\gamma_0^{Cross} = 0.02$  for Ni and Cu, which corresponds to an increase difficulty in cross slipping and cell formation for these materials. The model uses the same mesoscale parameters in Table 2 for modeling Cu and Ni, except for  $K_{struc} = 2.7$  and  $K_{struc} = 3$ , respectively.

Mesoscale parameters (Table 2) characterize the strain hardening induced by dislocation structures and they are attributes of the structure, not a material. Thus, the same parameters can be known *a priori* for various materials, without the need for recalibration, and reducing the number of unknown parameters. An analogous result was found for the parameterization of dislocation structures under monotonic loading (Dindarlou and Castelluccio, 2022), which was used to enrich data sets with proxy materials. If material-invariant parameters are characterized with single crystal data, they extend the predictive power even if only polycrystalline data is available (e. g., alloys).

The results in Fig. 13 demonstrate good agreement between the CSSC from simulations and experiments for Ni and Cu single crystals at room temperature. As expected from our prior work (Castelluccio and McDowell, 2017), the model captures Ni response, but notably, it employs the same mesoscale parameterization for Al. Similarly, the same model captures the response of Cu without any special provision except for the atomic process unit parameters in Table 4. The fitting to the experimental data could be further improved with a mathematical optimization approach that integrates data from various materials. However, we note that the uncertainty of the experiments, particularly single crystals, is unknown and it can be significant due to a number of factors (exact crystal orientation, contribution of impurities, loading conditions, etc.).

Fig. 14 presents the CSSC temperature dependence for [149]-oriented Ni and Cu crystal and demonstrates a remarkable agreement between models and experiments. The model slightly overestimates hardening close to half melting temperatures since there are no provisions for additional high temperature recovery mechanisms (e.g., dislocation climb). Nevertheless, the trends as well as the magnitude of peak stresses for both Ni and Cu single crystals agree well with experiments. We highlighted that the model is identical to that for Al, and only parameters related to atomic unit processes and  $f_{inf}^{PSB}$  are different (e.g., Table 2). Similarly, the only dependence on

**Table 4**

Summary of atomistic process unit parameters for Al, Ni and Cu estimated using yield stress data (F Ashraf and Castelluccio, 2021) and observed in experiments (Basinski et al., 1980; Tippelt et al., 1997; Kassner and Wall, 1999; Feaugas, 1999; Essmann and Mughrabi, 1979).

Material	$F_o$ (eV)	$s_o^t$ (MPa)	p	q	$y_s$ (nm)	$y_e$ (nm)
Ni	2	44	0.667	1.5	25	1.5
Cu	2.3	17	0.667	1.5	25	1.5

**Table 5**

Temperature dependent wall fraction for PSBs for Ni. Also,  $f_{inf}^{Lab} = \frac{1}{\sqrt{2}} f_{inf}^{PSB}$ .

Homologous temperature	0.045	0.17	0.35	0.43
$f_{inf}^{PSB}$ for Ni	0.24	0.23	0.22	0.21

**Table 6**

Temperature dependent wall fraction for PSBs for Cu. Also,  $f_{inf}^{Lab} = \frac{1}{\sqrt{2}} f_{inf}^{PSB}$ .

Homologous temperature	0.057	0.22	0.37	0.5
$f_{inf}^{PSB}$ for Cu	0.24	0.22	0.18	0.16

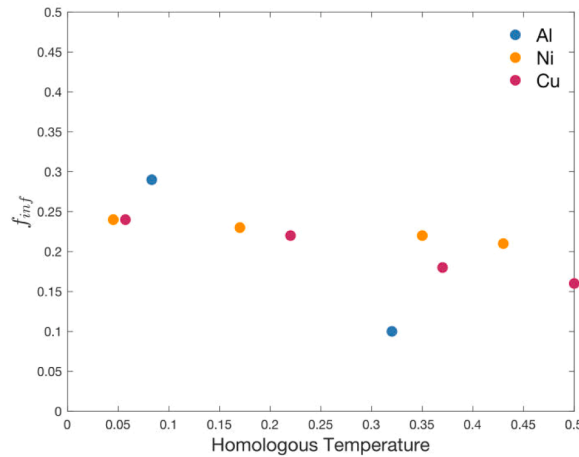


**Fig. 12.** Parameterization of the wall fraction at saturation for PSBs ( $f_{inf}^{PSB}$ ) in Al, Ni and Cu as a function of their corresponding homologous temperatures. These results resemble the experimental dependence of PSBs wall fraction shown in Fig. 4.

temperature is explicitly on the flow rule and in the wall volume fraction for PSBs (as suggested by TEM analysis).

To conclude the comparison with Ni and Cu, Fig. 15 presents the cyclic hardening curves for single-slip oriented Ni and Cu single crystals at 298 K from models and experiments. These results demonstrate that the history dependence introduced into the crystal plasticity to capture Al response (Fig. 1) also works for Ni and Cu.

**5. Discussion**

Much experimental research in the last 50 years has characterized the cyclic response of FCC single crystals over a wide range of temperatures. However, modeling have lagged and most approaches have been validated only with polycrystalline responses. Substructure-sensitive crystal plasticity approaches were initially proposed and validated (Castelluccio and McDowell, 2017) for Ni single- and poly-crystals under saturated conditions. However, our analysis demonstrated that this approach is inadequate for materials above 0.2 of the homologous temperature (e.g., Al at room temperature), which do not fully saturate due to the continuous evolution of dislocation structures. Hence, this work generalised our prior efforts to account for cyclic history and temperature.

Our prior work for monotonic loading (Dindarlou and Castelluccio, 2022) demonstrated that fitting models to polycrystals stress-strain curves does not guarantee good agreement with single crystal experiments. Similarly, we now consider the model for Al but assuming a constant  $\eta$ , which is equivalent to assuming  $l_{struc} \propto \frac{1}{\sqrt{\rho}}$  for all structures. We assume constant  $\eta = 2$  or 5 depending on the grain size (affecting the mean free path akin to Haouala et al. (2018)) to demonstrates in Fig. 16(a) a good agreement between modeling and experimental CSSC for polycrystals. However, the analysis of single crystals deformed along [123] and [001] directions in Fig. 16(b) confirms that constant  $\eta$  for different crystallographic orientations cannot predict single crystal cyclic responses. An  $\eta = 2$  overpredicts the response of both crystals while  $\eta = 5$  underpredicts some of them. Furthermore, Fig. 17 presents the von Mises stresses computed from all elements in the polycrystalline model with grain size of 200  $\mu\text{m}$  and an applied cyclic strain of 0.12%. These results demonstrate a different von Mises stress distributions from a variable or constant  $\eta$ , the later of which reduces it variability by a third.

The lack of agreement in Fig. 16(b) is ubiquitous in crystal plasticity models that are parameterized exclusively with polycrystalline data. These results demonstrate that tampering with crystal plasticity parameters to reproduce polycrystal experiments without

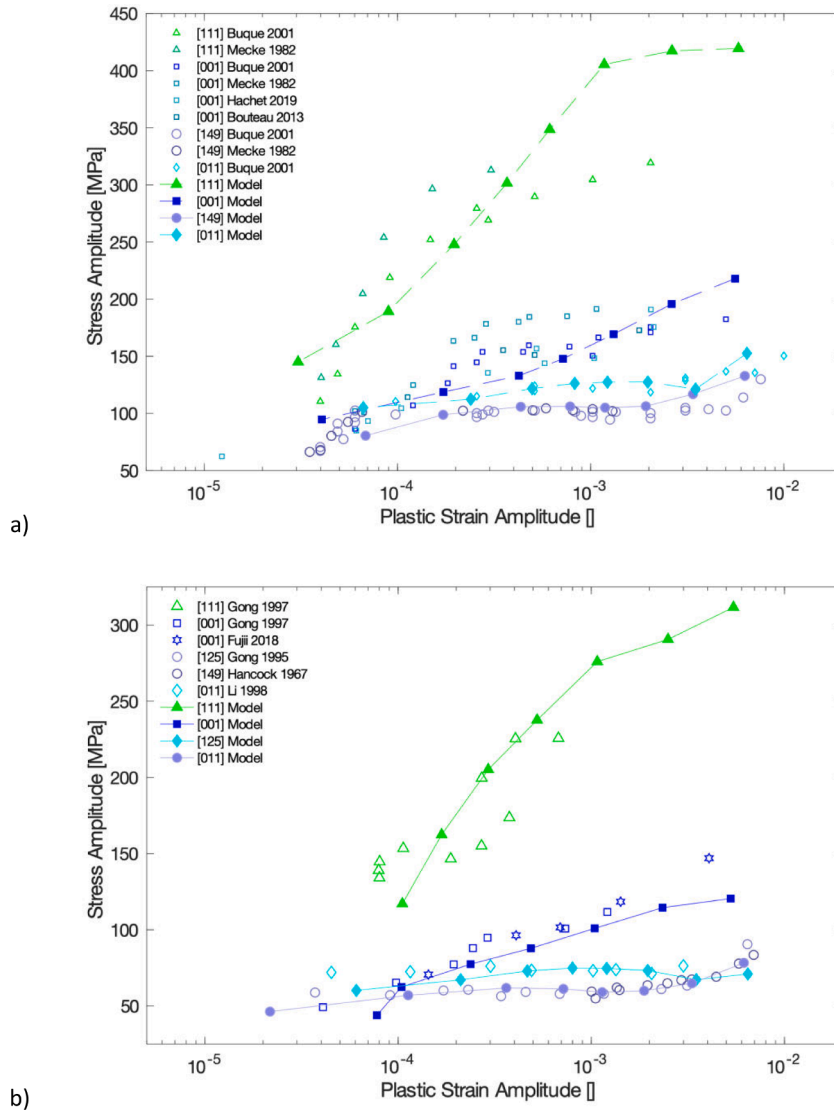


**Fig. 13.** Cyclic stress-strain response of a) Ni and b) single crystal oriented along [001, 149, 011], and [111] direction under fully reversed strain-controlled loading ( $R_e = -1$ ) at 298 K. Experimental data were compiled from (Hachet et al., 2020; Buque, 2001; Mecke and Blochwitz, 1982; Bouteau, 2013) for Ni and (Gong et al., 1997; Fujii et al., 2018; Gong et al., 1995; Hancock and Grosskreutz, 1969; Li et al., 1998) for Cu.

independent validation affects the mean response and its variability at the local crystal level. Notably, modeling error is largest for single crystals under single slip since they develop the most heterogeneous structures with the largest aspect ratios. This is particularly problematic for fatigue prognosis, in which cracks are more likely to initiate and propagate in single slip oriented grains. Hence, our modeling results partially explain the lack of success from models in predicting local cracking, which has often been attributed to the damage formulation (e.g., fatigue indicator parameter of preference) rather than the underlying constitutive response.

We argue that substructure-sensitive crystal plasticity predicts the response of single crystals thanks to the independent validation of mesoscale parameters, particularly the heterogeneous mean free path. Certainly, the correct prediction of substructure length scales is akin to validating the local stress thanks to the similitude principle. Other approaches based on dislocation densities or geometrically necessary dislocations (GNDs) carry larger experimental uncertainty, which are often of little value when translating into local stress error in simulations. In addition, polycrystalline samples affect the triaxial deformation state of grains and model validation requires a 3D rather a 2D representation. Hence, model comparisons with experiments should rely on single crystals or 3D characterization of grain ensembles rather than handpicking isolated grains.

We further demonstrated that the parameterization of dislocation substructures with the accumulation of cross slip shear strain can effectively predict the temperature dependence of initial and secondary hardening. Notably, temperature dependence of secondary hardening is entirely driven by cross slip activation and no additional parameterization is required. Similarly, cross slip strain accumulation also accounts for the prevalence of secondary hardening at higher strains or number of cycles without any additional



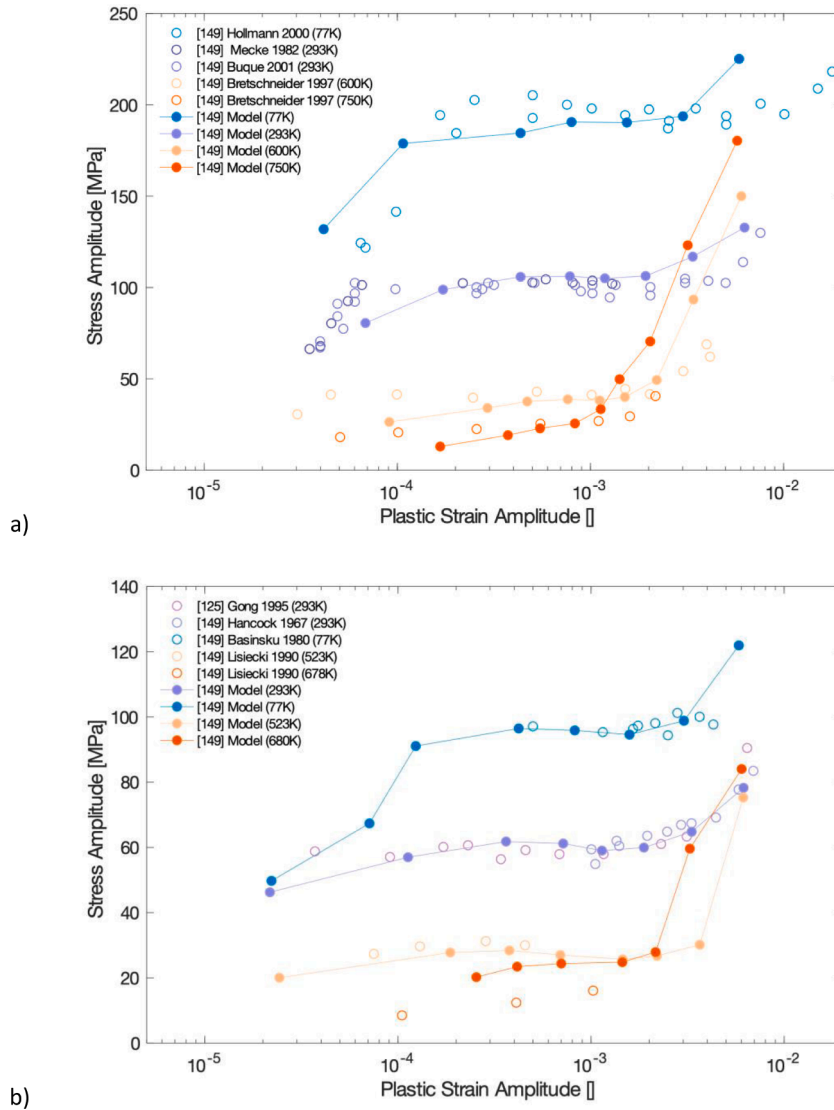


**Fig. 14.** Cyclic stress-strain response of [149] a) Ni and b) Cu single crystal under fully reversed strain-controlled loading ( $R_\epsilon = -1$ ) at various temperatures. Data from (Bretschneider et al., 1997; Buque, 2001; Hollmann et al., 2000) for Ni and (Basinski et al., 1980; Lisiecki and Weertman, 1990; Gong et al., 1995; Hancock and Grosskreutz, 1969) for Cu.

provision.

We demonstrated that substructure-sensitive models simplify parameter identification by sharing identical mesoscale parameters across FCC materials. Hence, modeling a new material requires identifying atomic unit processes parameters (Table 1), which can be estimated independently (Ashraf and Castelluccio, 2021) or through lower scale modeling (e.g., Molecular Dynamics) (Narayanan et al., 2014; Varvenne et al., 2017). As a result, this crystal plasticity approach is well posed to predict the cyclic response of single crystals for engineering materials such as austenitic stainless steels, for which no single crystal data are available. Secondly, the approach reproduces the cyclic response at various temperatures by introducing a single temperature dependence on the wall fraction of PSBs, directly informed by TEM (Ashraf and Castelluccio, 2021). Thirdly, the model presented here is identical (including atomic unit processes parameters) to that developed for monotonic loading except for the parameterization of  $\eta$  and  $f_w$  (Dindarlou and Castelluccio, 2022). Hence, the approach can work with experimental mesoscale parameterizations of  $\eta$  and  $f_w$  from various loading conditions—R ratio, overloads, strain rates, creep—which share similar dislocation structures (Lukas et al., 1999; Kiritani et al., 2002; Blum et al., 2014).

Experimental evidence suggests diverging responses of  $f_w$  depending on the loading conditions. This paper reconciled these notions by introducing Eqs. (17) and (18), which parameterize the evolution of  $f_w$  under monotonic or cyclic loading: Under monotonic loading ( $N = 1$ ), the wall fraction increases monotonically. Under saturated cyclic conditions, the reduction of the wall fraction with increasing cyclic plasticity (red line in Fig. 3) serves as a recovery mechanism for the back stress (Eq. (5)), which lacks a recovery term. This

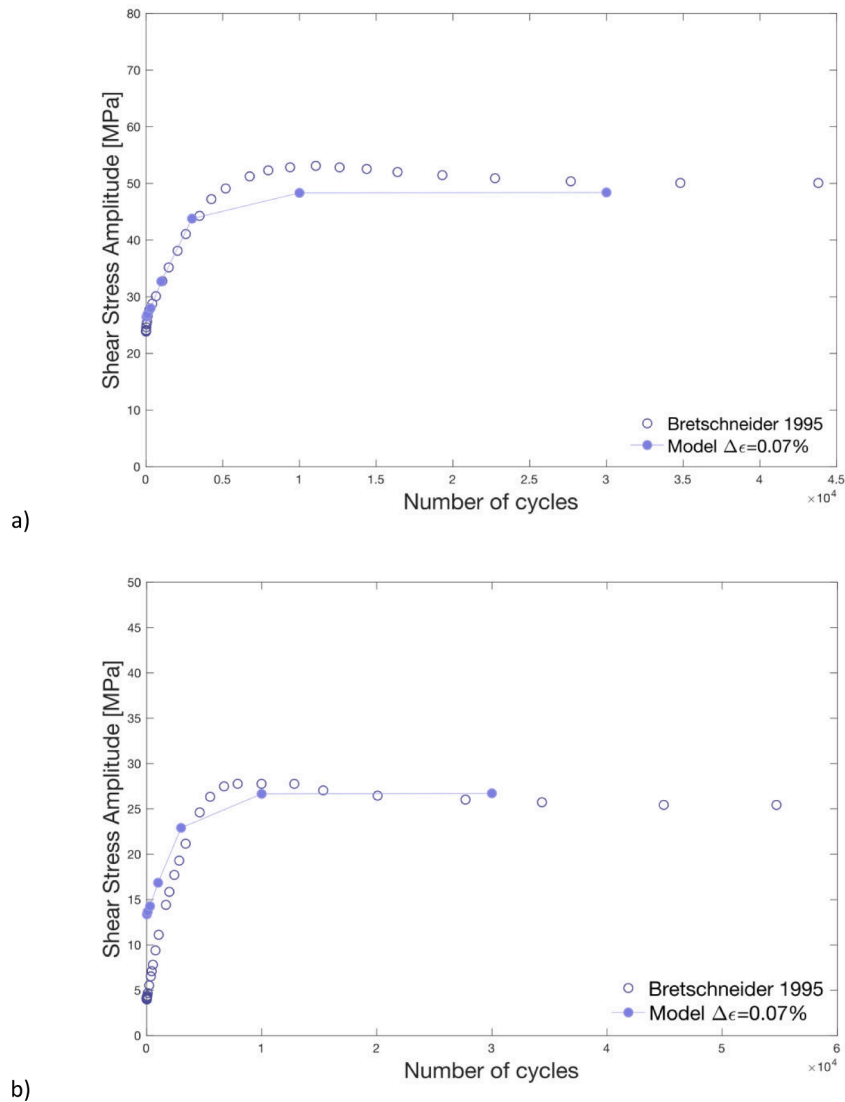


**Fig. 15.** Cyclic hardening of a) Ni and b) Cu single crystal oriented for single slip at 298 K. The experimental data corresponds to (Bretschneider et al., 1995; Magnin et al., 2001).

approach provides a physically-sound formulation for the back stress hardening and recovery balance, which has normally relied on phenomenological equations (e.g., Armstrong-Frederick, Ohno-Wang, etc.) (Hennessey et al., 2017).

This work also innovates with a novel formulation that accelerates the modeling under cyclic loading. Rather than explicitly applying thousands of cycles to predict the stress-strain response, the model defines the cycle number as an input parameter. This strategy accelerates the simulations while it can still be used to predict the cycle-by-cycle history by updating the cycle number parameter on every cycle (Fig. 7). As a result, the model is particularly useful to assess the likelihood of cracking throughout cyclic history by means of fatigue indicator parameters (Castelluccio et al., 2016; Kakandar et al., 2020) or microstructure-sensitive fatigue life analytical formulations (Ashraf et al., 2022).

To conclude, our analysis also bridges a gap in understanding the cyclic response of FCC materials. By considering material-invariant substructures at similar homologous temperature we can compare the cyclic response of various FCC metals as shown in Fig. 18. In this case, the experimental cyclic stresses are normalized by the shear modulus and the burgers vector divided by the structure spacing, which depends strongly on temperature. The agreement among different materials reinforces the value of substructure-sensitive crystal plasticity framework in predicting the mechanical response. It further demonstrates the potential of material-invariant parameters for mitigating the difficulties in identifying crystal plasticity parameters.

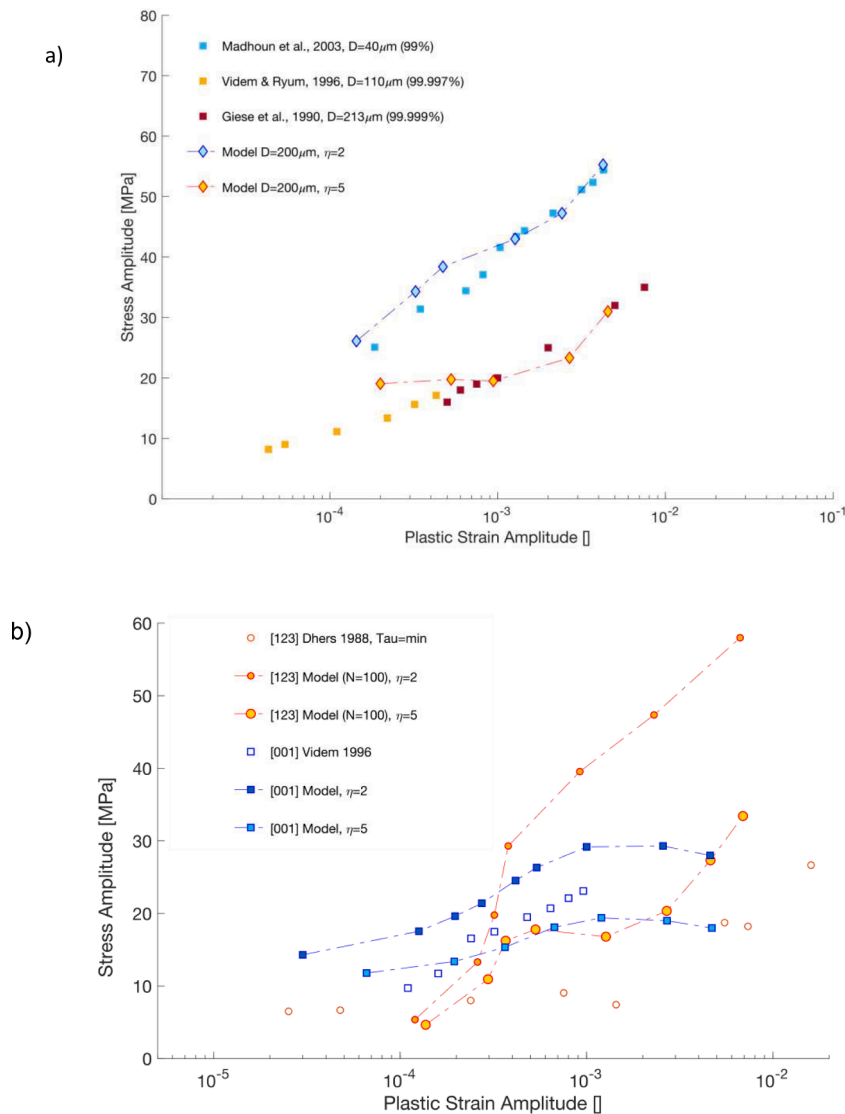


**Fig. 16.** a) Cyclic stress-strain response of Al polycrystals using constant  $\eta = 2$  or 5 depending on the grain size. b) Cyclic stress-strain response of Al single crystals deformed along [123] and [001] directions at 298 K using constant  $\eta = 2$  or 5.

## 6. Conclusions

This work bridges the gap in modeling cyclic deformation of single phase FCC single crystals using mesoscale substructure as material invariants. We proposed a novel methodology to quantify the effects of cyclic history on single- and poly-crystals and their corresponding cyclic response. The approach describes transients in dislocation structures to represent initial and secondary hardening up to 0.5 homologous temperature. We highlight that the number of cycles and the temperature affect the activation of cross slip, which is used to determine the dominant dislocation substructures and control hardening.

In terms of computational effort, this work innovates in physics-based engineering models by predicting the cyclic response under thousands and millions of cycles without explicitly applying them. We define the number of cycles as an input, and the model estimates the constitutive response for such cycle by quantifying the partition of plasticity across slip systems.

The work further generalizes the notion of mesoscale material-invariant parameters, which have now been shown to exist for modeling cyclic deformation. Hence, substructure-sensitive models can leverage from parameters calibrated for other materials with similar structures. This approach provides a more accurate prediction of single crystal response than just relying on parameters calibrated to polycrystalline experiments. In addition, it allows to estimate the cyclic response of different materials by changing only atomic unit process parameters. Ongoing efforts are focused on predicting the cyclic response of alloys that shows similar mesoscale dislocation substructures under cyclic loading.

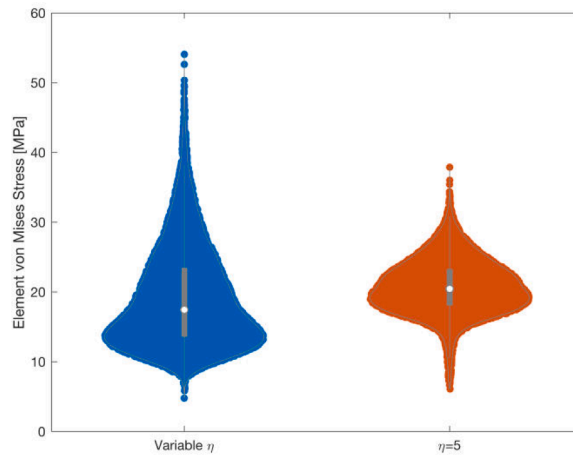


**Fig. 17.** Violin plots for the von Mises Stress from all elements in polycrystalline models using variable (Left) or constant (Right)  $\eta$  for a grain size of 200  $\mu\text{m}$  and an applied cyclic strain of 0.12%. Exact same mesh and grain distributions is used for both models.

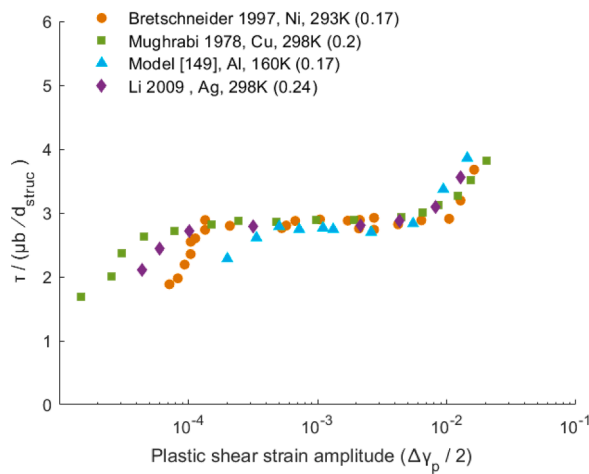


**Fig. 18.** Cyclic stress-strain response of Ni, Cu, Ag, and Al single crystals at the same homologous temperature, the y-axis is normalized with the bow-out stress (Brown, 2006).  $d_{struc}$  was estimated as the PSB wall spacing computed from TEM (Ashraf and Castelluccio, 2021).

**Declaration of Competing Interest**

The authors declare that they have no known competing financial interests or personal relationships that could have appeared to influence the work reported in this paper.

**Data Availability**

Data will be made available on request.

**Acknowledgement**

The authors are grateful for the support of The Punjab Educational Endowment Fund (PEEF) for funding the project. The corresponding author is grateful for the support from EPSRC, UK Grant EP/R034478/1.

**References**

Roters, F., Eisenlohr, P., Hantcherli, L., Tjahjanto, D.D., Bieler, T.R., Raabe, D., 2010. Overview of constitutive laws, kinematics, homogenization and multiscale methods in crystal plasticity finite-element modeling: theory, experiments, applications. *Acta Mater.* 58, 1152–1211. <https://doi.org/10.1016/j.actamat.2009.10.058>.

- Pokharel, R., Lind, J., Kanjarla, A.K., Lebensohn, R.A., Li, S.F., Kenesei, P., et al., 2014. Polycrystal Plasticity: comparison Between Grain - Scale Observations of Deformation and Simulations. *Annu. Rev. Condens. Matter Phys.* 5, 317–346. <https://doi.org/10.1146/annurev-conmatphys-031113-133846>.
- Sangid, M.D., 2019. Coupling in situ experiments and modeling – Opportunities for data fusion, machine learning, and discovery of emergent behavior. *Curr. Opin. Solid State Mater. Sci.*, 100797 <https://doi.org/10.1016/j.cossms.2019.100797>.
- Roy, C.J., Oberkampf, W.L., 2011. A comprehensive framework for verification, validation, and uncertainty quantification in scientific computing. *Comput. Methods Appl. Mech. Eng.* 200, 2131–2144. <https://doi.org/10.1016/j.cma.2011.03.016>.
- El Shawish, S., Cizek, L., 2017. Combining Single- and Poly-Crystalline Measurements for Identification of Crystal Plasticity Parameters: application to Austenitic Stainless Steel. *cryst.* 7, 181. <https://doi.org/10.3390/cryst7060181>.
- Pirgazi, H., Kestens, L.A.I., 2021. Semi in-situ observation of crystal rotation during cold rolling of commercially pure aluminum. *Mater. Charact.* 171, 110752 <https://doi.org/10.1016/j.matchar.2020.110752>.
- Rovinelli, A., Guilhem, Y., Proudhon, H., Lebensohn, R.A., Ludwig, W., Sangid, M.D., 2017. Assessing reliability of fatigue indicator parameters for small crack growth via a probabilistic framework. *Model. Simul. Mater. Sci. Eng.* 25, 045010 <https://doi.org/10.1088/1361-651X/aa6c45>.
- Ashraf, F., Cini, A., Castelluccio, G.M., 2022. Analytical fatigue life formulation for notches informed by crystal plasticity. *Int. J. Fatigue* 163, 107072. <https://doi.org/10.1016/j.ijfatigue.2022.107072>.
- Sedighiani, K., Traka, K., Roters, F., Raabe, D., Sietsma, J., Diehl, M., 2022. Determination and analysis of the constitutive parameters of temperature-dependent dislocation-density-based crystal plasticity models. *Mech. Mater.* 164, 104117 <https://doi.org/10.1016/j.mechmat.2021.104117>.
- Herrera-Solaz, V., LLorca, J., Dogan, E., Karaman, I., Segurado, J., 2014. An inverse optimization strategy to determine single crystal mechanical behavior from polycrystal tests: application to AZ31 Mg alloy. *Int. J. Plast.* 57, 1–15. <https://doi.org/10.1016/j.ijplas.2014.02.001>.
- Estrin, Y., Brechet, Y., Braasch, H., 1996. A Dislocation Density Based Constitutive Model for Cyclic Deformation. *J. Eng. Mater. Technol.* 118, 441–447. <https://doi.org/10.1115/1.2805940>.
- Estrin, Y., Tóth, L.S., Molinari, A., Bréchet, Y., 1998. A dislocation-based model for all hardening stages in large strain deformation. *Acta Mater.* 46, 5509–5522. [https://doi.org/10.1016/S1359-6454\(98\)00196-7](https://doi.org/10.1016/S1359-6454(98)00196-7).
- Sedláček, R., Blum, W., 2002. Microstructure-based constitutive law of plastic deformation. *Comput. Mater. Sci.* 25, 200–206. [https://doi.org/10.1016/S0927-0256\(02\)00264-1](https://doi.org/10.1016/S0927-0256(02)00264-1).
- Brahme, A.P., Inal, K., Mishra, R.K., Saimoto, S., 2011. The backstress effect of evolving deformation boundaries in FCC polycrystals. *Int. J. Plast.* 27, 1252–1266. <https://doi.org/10.1016/j.ijplas.2011.02.006>.
- Steckmeyer, A., Sauzay, M., Weidner, A., Hieckmann, E., 2012. Micromechanical modelling of the cyclic stress–strain behaviour of nickel polycrystals. *Int. J. Fatigue* 40, 154–167. <https://doi.org/10.1016/j.ijfatigue.2011.10.019>.
- Sauzay, M., Liu, J., Rachdi, F., Signor, L., Ghidossi, T., Villechaise, P., 2014. Physically-Based Simulations of the Cyclic Behavior of FCC Polycrystals. *Adv. Mat. Res.* 891–892, 833–839. <https://doi.org/10.4028/www.scientific.net/AMR.891-892.833>.
- Castelluccio, G.M., McDowell, D.L., 2017. Mesoscale cyclic crystal plasticity with dislocation substructures. *Int. J. Plast.* 98, 1–26. <https://doi.org/10.1016/j.ijplas.2017.06.002>.
- Sauzay, M., Kubin, L.P., 2011. Scaling laws for dislocation microstructures in monotonic and cyclic deformation of fcc metals. *Prog. Mater. Sci.* 56, 725–784. <https://doi.org/10.1016/j.pmatsci.2011.01.006>.
- Nakanishi, Y., Tanaka, H., Fujii, T., Onaka, S., Kato, M., 2013. Low-temperature fatigue behaviour and development of dislocation structure in aluminium single crystals with single-slip orientation. *Philos. Mag.* 93, 2759–2768. <https://doi.org/10.1080/14786435.2013.786193>.
- Dindarlou, S., Castelluccio, G.M., 2022. Substructure-sensitive crystal plasticity with material-invariant parameters. *Int. J. Plast.*, 103306 <https://doi.org/10.1016/j.ijplas.2022.103306>.
- Li, P., Li, S.X., Wang, Z.G., Zhang, Z.F., 2011. Fundamental factors on formation mechanism of dislocation arrangements in cyclically deformed fcc single crystals. *Prog. Mater. Sci.* 56, 328–377. <https://doi.org/10.1016/j.pmatsci.2010.12.001>.
- Pham, M.S., Holdsworth, S.R., Janssens, K.G.F., Mazza, E., 2013. Cyclic deformation response of AISI 316 L at room temperature: mechanical behaviour, microstructural evolution, physically-based evolutionary constitutive modelling. *Int. J. Plast.* 47, 143–164. <https://doi.org/10.1016/j.ijplas.2013.01.017>.
- Picak, S., Wegener, T., Sajadifar, S.V., Sobrero, C., Richter, J., Kim, H., et al., 2021. On the low-cycle fatigue response of CoCrNiFeMn high entropy alloy with ultra-fine grain structure. *Acta Mater.* 205, 116540 <https://doi.org/10.1016/J.ACTAMAT.2020.116540>.
- Charsley, P., Bangert, U., Appleby, L.J., 1989. The effect of temperature and amplitude on dislocation structures in cyclically deformed pure aluminium. *Mater. Sci. Eng. A* 113, 231–236. [https://doi.org/10.1016/0921-5093\(89\)90311-0](https://doi.org/10.1016/0921-5093(89)90311-0).
- Videm, M., Ryum, N., 1996a. Cyclic deformation of [001]aluminium single crystals. *Mater. Sci. Eng. A* 219, 1–10. [https://doi.org/10.1016/S0921-5093\(96\)10261-6](https://doi.org/10.1016/S0921-5093(96)10261-6).
- Kassner, M.E., Wall, M.A., MA, Delos-Reyes, 1997. Microstructure and mechanisms of cyclic deformation of aluminium single crystals at 77 K. *Metall. Mater. Trans. A* 28 A, 595–609. <https://doi.org/10.1007/s11661-997-0045-2>.
- Holzwarth, U., Essmann, U., 1993. Transformation of dislocation patterns in fatigued copper single crystals. *Mater. Sci. Eng. A* 164, 206–210. [https://doi.org/10.1016/0921-5093\(93\)90663-Y](https://doi.org/10.1016/0921-5093(93)90663-Y).
- Basinski, Z.S., Korbel, A.S., Basinski, S.J., 1980. The temperature dependence of the saturation stress and dislocation substructure in fatigued copper single crystals. *Acta Metall.* 28, 191–207. [https://doi.org/10.1016/0001-6160\(80\)90068-1](https://doi.org/10.1016/0001-6160(80)90068-1).
- Tippelt, B., Bretschneider, J., Hähner, P., 1997. The dislocation microstructure of cyclically deformed nickel single crystals at different temperatures. *Physica Status Solidi A Appl. Res.* 163, 11–26. [https://doi.org/10.1002/1521-396X\(199709\)163:1<11::AID-PSSA11>3.0.CO;2-X](https://doi.org/10.1002/1521-396X(199709)163:1<11::AID-PSSA11>3.0.CO;2-X).
- Vorren, O., Ryum, N., 1988. Cyclic deformation of Al single crystals: effect of the crystallographic orientation. *Acta Metall.* 36, 1443–1453. [https://doi.org/10.1016/0001-6160\(88\)90212-X](https://doi.org/10.1016/0001-6160(88)90212-X).
- Vorren, O., Ryum, N., 1987. Cyclic deformation of Al-single crystals at low constant plastic strain amplitudes. *Acta Metall.* 35, 855–866. [https://doi.org/10.1016/0001-6160\(87\)90162-3](https://doi.org/10.1016/0001-6160(87)90162-3).
- Giese, A., Estrin, Y., 1993. Mechanical behaviour and microstructure of fatigued aluminium single crystals. *Scripta Metallurgica et Materiala* 28, 803–807. [https://doi.org/10.1016/0956-716X\(93\)90356-W](https://doi.org/10.1016/0956-716X(93)90356-W).
- Mughrabi, H., 1978. The cyclic hardening and saturation behaviour of copper single crystals. *Mater. Sci. Eng. R Rep.* 33, 207–223. [https://doi.org/10.1016/0025-5416\(78\)90174-X](https://doi.org/10.1016/0025-5416(78)90174-X).
- Rie, K.-T., 1987. *Low Cycle Fatigue and Elasto-Plastic Behaviour of Materials*. editor. Springer Netherlands, Dordrecht. <https://doi.org/10.1007/978-94-009-3459-7>.
- Polak, J., Helesic, J., Obrtlík, K., 1988. Nucleation stress for persistent slip bands in fatigued copper single crystals. *Mater. Sci. Eng. R Rep.* 101, 7–12. [https://doi.org/10.1016/0025-5416\(88\)90786-0](https://doi.org/10.1016/0025-5416(88)90786-0).
- Wang, R., Mughrabi, H., 1984. Secondary cyclic hardening in fatigued copper monocrystals and polycrystals. *Mater. Sci. Eng. R Rep.* 63, 147–163.
- Lisiecki, L.L., Weertman, J.R., 1990. Orientation effects on the elevated temperature fatigue of copper single crystals. *Acta Metall. Mater.* 38, 509–519. [https://doi.org/10.1016/0956-7151\(90\)90157-C](https://doi.org/10.1016/0956-7151(90)90157-C).
- Fougeres, R., 1993. Early stages of fatigue damage in aluminium and aluminium alloys. *Le Journal de Physique IV* 03. <https://doi.org/10.1051/jp4:19937106>. C7-669-C7-678.
- Bretschneider, J., Holste, C., Tippelt, B., 1997. Cyclic plasticity of nickel single crystals at elevated temperatures. *Acta Mater.* 45, 3775–3783. [https://doi.org/10.1016/S1359-6454\(97\)00030-X](https://doi.org/10.1016/S1359-6454(97)00030-X).
- Obrtlík, K., Kruml, T., Polák, J., 1994. Dislocation structures in 316L stainless steel cycled with plastic strain amplitudes over a wide interval. *Mater. Sci. Eng. A* 187, 1–9. [https://doi.org/10.1016/0921-5093\(94\)90325-5](https://doi.org/10.1016/0921-5093(94)90325-5).
- Mitchell, A.B., Teer, D.G., 1970. The analysis of dislocation structures in fatigued aluminium single crystals exhibiting striations. *Philos. Mag.* 22, 399–417. <https://doi.org/10.1080/14786437008228233>.
- Dhers, J., Driver, J., 1988. The cyclic response and microstructure of aluminium single crystal. In: In: Lukáš P, Polak J editors *B Mechanisms in Fatigue of metals*, editor. Materials science Monographs. Elsevier, Amsterdam, pp. 33–40.

- Kocks, U.F., Argon, A.S., Ashby, M.F., 1975. *Thermodynamics and Kinetics of Slip*, 53. Pergamon Press.
- Mura, R., Ting, T.C.T., 1989. Micromechanics of Defects in Solids (2nd rev. ed.). *J. Appl. Mech.* 56, 487–488. <https://doi.org/10.1115/1.3176116>.
- Wang, H., Capolungo, L., Clausen, B., Tomé, C.N., 2017. A crystal plasticity model based on transition state theory. *Int. J. Plast.* 93, 251–268. <https://doi.org/10.1016/j.ijplas.2016.05.003>.
- Sedighiani, K., Diehl, M., Traka, K., Roters, F., Sietsma, J., Raabe, D., 2020. An efficient and robust approach to determine material parameters of crystal plasticity constitutive laws from macro-scale stress–strain curves. *Int. J. Plast.* 134, 102779 <https://doi.org/10.1016/j.ijplas.2020.102779>.
- Devincere, B., Hoc, T., Kubin, L., 2008. Dislocation mean free paths and strain hardening of crystals. *Science* 320, 1745–1748. <https://doi.org/10.1126/science.1156101>.
- Alhamany, A., Chicois, J., Fougères, R., Hamel, A., 1992. Effet Bauschinger lors de la plasticité cyclique de l'aluminium pur monocristallin. *J. Phys. III* 2, 1491–1508. <https://doi.org/10.1051/jp3:1992195>.
- Suresh, S., 1998. *Fatigue of Materials*, 2nd ed. Cambridge University Press. <https://doi.org/10.1017/cbo9780511806575>.
- Hecker, M., Thiele, E., Holste, C., 1997. X-ray diffraction analysis of internal stresses in the dislocation structure of cyclically deformed nickel single crystals. *Mater. Sci. Eng. A* 234–236, 806–809. [https://doi.org/10.1016/s0921-5092\(97\)00370-5](https://doi.org/10.1016/s0921-5092(97)00370-5).
- Varshni, Y.P., 1970. Temperature dependence of the elastic constants. *Phys. Rev. B* 2, 3952–3958. <https://doi.org/10.1103/PhysRevB.2.3952>.
- Ashraf, F., Castelluccio, G.M., 2021a. A robust approach to parameterize dislocation glide energy barriers in FCC metals and alloys. *J. Mater. Sci.* 56, 16491–16509. <https://doi.org/10.1007/s10853-021-06376-1>.
- Langer, J.S., Bouchbinder, E., Lookman, T., 2010. Thermodynamic theory of dislocation-mediated plasticity. *Acta Mater.* 58, 3718–3732. <https://doi.org/10.1016/j.actamat.2010.03.009>.
- Kassner, M.E., Wall, M.A., 1999. Microstructure and mechanisms of cyclic deformation in aluminum single crystals at 77 K: part II. Edge dislocation dipole heights. *Metall. Mater. Trans. A* 30, 777–779. <https://doi.org/10.1007/s11661-999-0069-x>.
- Feaugas, X., 1999. On the origin of the tensile flow stress in the stainless steel AISI 316 L at 300 K: back stress and effective stress. *Acta Mater.* 47, 3617–3632. [https://doi.org/10.1016/S1359-6454\(99\)00222-0](https://doi.org/10.1016/S1359-6454(99)00222-0).
- Essmann, U., Mughrabi, H., 1979. Annihilation of dislocations during tensile and cyclic deformation and limits of dislocation densities. *Philos. Mag. A* 40, 731–756. <https://doi.org/10.1080/01418617908234871>.
- Kubin, L., Devincere, B., Hoc, T., 2008. Modeling dislocation storage rates and mean free paths in face-centered cubic crystals. *Acta Mater.* 56, 6040–6049. <https://doi.org/10.1016/j.actamat.2008.08.012>.
- Fivel, M., Tabourot, L., Rauch, E., Canova, G., 1998. Identification through mesoscopic simulations of macroscopic parameters of physically based constitutive equations for the plastic behaviour of fcc single crystals. *J. De Physique IV: JP* 8, 151–158. <https://doi.org/10.1051/jp4:1998819>.
- Schwartz, J., Fandeur, O., Rey, C., 2013. Numerical approach of cyclic behaviour of 316LN stainless steel based on a polycrystal modelling including strain gradients. *Int. J. Fatigue* 55, 202–212. <https://doi.org/10.1016/j.ijfatigue.2013.07.003>.
- Madee, R., Devincere, B., Kubin, L., Hoc, T., Rodney, D., 2003. The role of collinear interaction in dislocation-induced hardening. *Science* 301, 1879–1882. <https://doi.org/10.1126/science.1085477>.
- Grosskreutz, C.J., Mughrabi, H., 1975. *Description of the Work-Hardened Structure at Low Temperature in Cyclic Deformation. Constitutive Equations in Plasticity*. The MIT Press, Cambridge, Mass, pp. 251–326, 1st Edition edition.
- Hachet, G., Oudriss, A., Barnoush, A., Millet, R., Wan, D., Metsue, A., et al., 2020. The influence of hydrogen on cyclic plasticity of <001>-oriented nickel single crystal. Part I: dislocation organisations and internal stresses. *Int. J. Plast.* 126 <https://doi.org/10.1016/j.ijplas.2019.09.017>.
- Szajewski, B.A., Pavia, F., Curtin, W.A., 2015. Robust atomistic calculation of dislocation line tension. *Modell. Simul. Mater. Sci. Eng.* 23 <https://doi.org/10.1088/0965-0393/23/8/085008>.
- Tabata, T., Fujita, H., Hiraoka, M.A., Miyake, S., 1982. The relationship between flow stress and dislocation behaviour in [111]aluminium single crystals. *Philosophical Magazine A: Physics of Condensed Matter, Structure, Defects and Mechanical Properties* 46, 801–816. <https://doi.org/10.1080/01418618208236932>.
- Armstrong, R.W., Rodriguez, P., 2006. Flow stress/strain rate/grain size coupling for fcc nanopolycrystals. *Philos. Mag.* 86, 5787–5796. <https://doi.org/10.1080/14786430600764872>.
- Tabata, T., Yamanaka, S., Fujita, H., 1978. In situ deformation of the [111]aluminum single crystals observed by high voltage electron microscopy. *Acta Metall.* 26, 405–411. [https://doi.org/10.1016/0001-6160\(78\)90167-0](https://doi.org/10.1016/0001-6160(78)90167-0).
- Ashraf, F., Castelluccio, G.M., 2021b. On the Similitude Relation for Dislocation Wall Thickness under Cyclic Loading. *Mater. Sci. Engin. A* 840, 142972. <https://doi.org/10.1016/j.msea.2022.142972>.
- Oudriss, A., Feaugas, X., 2016. Length scales and scaling laws for dislocation cells developed during monotonic deformation of (001) nickel single crystal. *Int. J. Plast.* 78, 187–202. <https://doi.org/10.1016/j.ijplas.2015.11.003>.
- Hähner, P., Tippelt, B., Holste, C., 1998. On the dislocation dynamics of persistent slip bands in cyclically deformed F.C.C. metals. *Acta Mater.* 46, 5073–5084. [https://doi.org/10.1016/S1359-6454\(98\)00161-X](https://doi.org/10.1016/S1359-6454(98)00161-X).
- Boehme, F., Hidaka, K., Weertman, J.R., 1990. PSB observation in copper fatigued at one half the melting temperature. *Scripta Metallurgica et Materiala* 24, 2341–2346. [https://doi.org/10.1016/0956-716X\(90\)90090-4](https://doi.org/10.1016/0956-716X(90)90090-4).
- Li, P., Zhang, Z.F., Li, X.W., Li, S.X., Wang, Z.G., 2009. Effect of orientation on the cyclic deformation behavior of silver single crystals: comparison with the behavior of copper and nickel single crystals. *Acta Mater.* 57, 4845–4854. <https://doi.org/10.1016/j.actamat.2009.06.048>.
- Spätig, P., Heczko, M., Kruml, T., Seifert, H.P., 2018. Influence of mean stress and light water reactor environment on fatigue life and dislocation microstructures of 316 L austenitic steel. *J. Nucl. Mater.* 509, 15–28. <https://doi.org/10.1016/j.jnucmat.2018.05.064>.
- Li, P., Li, S.X., Wang, Z.G., Zhang, Z.F., 2010. Dislocation arrangements in cyclically deformed Au single crystal. *Mater. Sci. Eng. A* 527, 6244–6247. <https://doi.org/10.1016/j.msea.2010.06.040>.
- ABAQUS, 2017. *FEM Software V2017*. Simulia Corp., Providence, RI, USA.
- Groeber, M.A., Jackson, M.A., 2014. DREAM.3D: a digital representation environment for the analysis of microstructure in 3D. *Integr. Mater. Manuf. Innov.* 3, 56–72. <https://doi.org/10.1186/2193-9772-3-5>.
- Castelluccio, G.M., McDowell, D.L., 2015. Microstructure and mesh sensitivities of mesoscale surrogate driving force measures for transgranular fatigue cracks in polycrystals. *Mater. Sci. Eng. A Struct. Mater.* 639, 626–639. <https://doi.org/10.1016/j.msea.2015.05.048>.
- Wang, J., Zhu, Z.G., Fang, Q.F., Liu, G.D., 1999. Influence of the crystallographic orientation on the behavior of fatigue in Al single crystals. *Mater. Res. Bull.* 34, 407–413. [https://doi.org/10.1016/S0025-5408\(99\)00024-0](https://doi.org/10.1016/S0025-5408(99)00024-0).
- Fujii, T., Uju, S., Tanaka, H., Murayama, T., Watanabe, C., Onaka, S., et al., 2008. *Plasticity, failure and fatigue in Structural Materials from Macro to Nano*. Hsia KJ, M.Göken, Pollock T, Portella PD, Moody NR, editors. In: Proc. of the Hael Mughrabi Honorary Symposium. The Minerals, Metals & Material Society, Warrendale, Pa, p. 123.
- Videm, M., Ryum, N., 1996b. Cyclic deformation and fracture of pure aluminium polycrystals. *Mater. Sci. Eng. A* 219, 11–20. [https://doi.org/10.1016/S0921-5093\(96\)10262-8](https://doi.org/10.1016/S0921-5093(96)10262-8).
- Tsou, J.C., Quesnel, D.J., 1982. Internal stress measurements during the saturation fatigue of polycrystalline aluminum. *Mater. Sci. Eng. R Rep.* 56, 289–299. [https://doi.org/10.1016/0025-5416\(82\)90105-7](https://doi.org/10.1016/0025-5416(82)90105-7).
- Giese, A., Styczynski, A., Estrin, Y., 1990. Cyclic hardening behaviour of polycrystalline aluminium under tension-compression. *Mater. Sci. Eng. A* 124, 13–15. [https://doi.org/10.1016/0921-5093\(90\)90160-5](https://doi.org/10.1016/0921-5093(90)90160-5).
- El-Madhoun, Y., Mohamed, A., Bassim, M.N., 2003. Cyclic stress-strain response and dislocation structures in polycrystalline aluminum. *Mater. Sci. Eng. A* 359, 220–227. [https://doi.org/10.1016/S0921-5093\(03\)00347-2](https://doi.org/10.1016/S0921-5093(03)00347-2).
- Bretschneider, J., Holste, C., Kleinert, W., 1995. Mechanical behaviour and development of dislocation arrangements of f.c.c. single crystals fatigued at 77 K. *Mater. Sci. Eng. A* 191, 61–72. [https://doi.org/10.1016/0921-5093\(94\)09626-8](https://doi.org/10.1016/0921-5093(94)09626-8).



- Buque, C., 2001. Dislocation structures and cyclic behaviour of [011] and  $[1\bar{1}1]$ -oriented nickel single crystals. *Int. J. Fatigue* 23, 671–678. [https://doi.org/10.1016/S0142-1123\(01\)00032-9](https://doi.org/10.1016/S0142-1123(01)00032-9).
- Mecke, K., Blochwitz, C., 1982. Saturation Dislocation Structures in Cyclically Deformed Nickel Single Crystals of Different Orientations. *Cryst. Res. Technol.* 17, 743–758. <https://doi.org/10.1002/crat.2170170610>.
- Bouteau, G., 2013. Etude De La Microstructure Et De La Concentration De Lacunes Dans Le Nickel Monocristallin Déformé En Fatigue. Université de La Rochelle.
- Gong, B., Wang, Z., Wang, Z., 1997. Cyclic deformation behavior and dislocation structures of [001] copper single crystals - I cyclic stress-strain response and surface feature. *Acta Mater.* 45, 1365–1377. [https://doi.org/10.1016/S1359-6454\(96\)00288-1](https://doi.org/10.1016/S1359-6454(96)00288-1).
- Fujii, T., Kajita, T., Miyazawa, T., Arai, S., 2018. Characterization of dislocation microstructures in cyclically deformed [001] copper single crystals using high voltage scanning transmission electron microscopy. *Mater. Charact.* 136, 206–211. <https://doi.org/10.1016/j.matchar.2017.12.026>.
- Gong, B., Wang, Z.G., Zhang, Y.W., 1995. The cyclic deformation behavior of Cu single crystal oriented for double slip. *Mater. Sci. Eng. A* 194, 171–178. [https://doi.org/10.1016/0921-5093\(94\)09662-7](https://doi.org/10.1016/0921-5093(94)09662-7).
- Hancock, J.R., Grosskreutz, J.C., 1969. Mechanisms of fatigue hardening in copper single crystals. *Acta Metall.* 17, 77–97. [https://doi.org/10.1016/0001-6160\(69\)90130-8](https://doi.org/10.1016/0001-6160(69)90130-8).
- Li, X.W., Wang, Z.G., Li, G.Y., Wu, S.D., Li, S.X., 1998. Cyclic stress-strain response and surface deformation features of [011] multiple-slip-oriented copper single crystals. *Acta Mater.* 46, 4497–4505. [https://doi.org/10.1016/S1359-6454\(98\)00151-7](https://doi.org/10.1016/S1359-6454(98)00151-7).
- Hollmann, M., Bretschneider, J., Holste, C., 2000. Dislocation structure and strain localization in nickel single crystals cyclically deformed at 77 K. *Cryst. Res. Technol.* 35, 479–492. [https://doi.org/10.1002/1521-4079\(200004\)35:4<479::AID-CRAT479>3.0.CO;2-E](https://doi.org/10.1002/1521-4079(200004)35:4<479::AID-CRAT479>3.0.CO;2-E).
- Magnin, T., Bosch, C., Wolski, K., Delafosse, D., 2001. Cyclic plastic deformation behaviour of Ni single crystals oriented for single slip as a function of hydrogen content. *Mater. Sci. Eng. A* 314, 7–11. [https://doi.org/10.1016/S0921-5093\(00\)01920-1](https://doi.org/10.1016/S0921-5093(00)01920-1).
- Haouala, S., Segurado, J., Llorca, J., 2018. An analysis of the influence of grain size on the strength of FCC polycrystals by means of computational homogenization. *Acta Mater.* 148, 72–85. <https://doi.org/10.1016/j.actamat.2018.01.024>.
- Narayanan, S., McDowell, D.L., Zhu, T., 2014. Crystal Plasticity Model for BCC Iron Atomistically Informed by Kinetics of Correlated Kinkpair Nucleation on Screw Dislocation. *J. Mech. Phys. Solids* 65, 54–68. <https://doi.org/10.1016/j.jmps.2014.01.004>.
- Varvenne, C., Leyson, G.P.M., Ghazisaeidi, M., Curtin, W.A., 2017. Solute strengthening in random alloys. *Acta Mater.* 124, 660–683. <https://doi.org/10.1016/j.actamat.2016.09.046>.
- Lukas, P., Kunz, L., Svoboda, M., 1999. Stress-strain response and fatigue life of copper single crystals cyclically loaded with a positive mean stress. *Mater. Sci. Eng. A* 272, 31–37.
- Kiritani, M., Sota, T., Tawara, T., Arimura, H., Yasunaga, K., Matsukawa, Y., et al., 2002. Defect Structures Introduced in FCC Metals by High-speed Deformation. *Radiat. Eff. Defects Solids* 157, 53–74. <https://doi.org/10.1080/10420150211397>.
- Blum, W., Dvořák, J., Král, P., Eisenlohr, P., Sklenička, V., 2014. Effect of grain refinement by ECAP on creep of pure Cu. *Mater. Sci. Eng. A Struct. Mater.* 590, 423–432. <https://doi.org/10.1016/j.msea.2013.10.022>.
- Hennessey, C., Castelluccio, G.M., McDowell, D.L., 2017. Sensitivity of polycrystal plasticity to slip system kinematic hardening laws for Al 7075-T6. *Mater. Sci. Eng. A Struct. Mater.* 687, 241–248. <https://doi.org/10.1016/j.msea.2017.01.070>.
- Castelluccio, G.M., Musinski, W.D., McDowell, D.L., 2016. Computational micromechanics of fatigue of microstructures in the HCF–VHCF regimes. *Int. J. Fatigue* 93 (Part 2), 387–396. <https://doi.org/10.1016/j.ijfatigue.2016.05.019>.
- Kakandar, E., Barrios, A., Michler, J., Maeder, X., Pierron, O.N., Castelluccio, G.M., 2020. A computational and experimental comparison on the nucleation of fatigue cracks in statistical volume elements. *Int. J. Fatigue* 137, 105633. <https://doi.org/10.1016/j.ijfatigue.2020.105633>.
- Brown, L.M., 2006. Dislocation bowing and passing in persistent slip bands. *Philos. Mag.* 86, 4055–4068. <https://doi.org/10.1080/14786430500501689>.

2022-12-06

# History and temperature dependent cyclic crystal plasticity model with material-invariant parameters

Ashraf, Farhan

Elsevier

---

Ashraf F, Castelluccio M. (2023) History and temperature dependent cyclic crystal plasticity model with material-invariant parameters. *International Journal of Plasticity*, Volume 161, February 2023, Article number 103494

<https://doi.org/10.1016/j.ijplas.2022.103494>

*Downloaded from Cranfield Library Services E-Repository*